A New Proposal to Jefferson Lab PAC-23

Measurement of Single Target-Spin Asymmetry in Semi-Inclusive Pion Electroproduction on a Transversely Polarized ^{3}He Target

The Jefferson Lab Hall A Collaboration

K. Wijesooriya
Argonne National Laboratory, Argonne, Illinois.

D.J. Margaziotis
California State University–Los Angles, Los Angeles, California.

D. Dutta, H. Gao, L. Zhu, W. Xu
Duke University, Durham, North Carolina.

B. Milbrath
Eastern Kentucky University, Richmond, Kentucky.

P. Markowitz
Florida International University, Miami, Florida.

M. Grosse-Perdekamp, H. Hiejima, A. Nathan, N. Makins, J.-C. Peng (Co-Spokesperson)
University of Illinois, Urbana-Champaign, Illinois.

A. Afanasev, J.-P. Chen (Co-Spokesperson), E. Chudakov, R. Feuerbach, J. Gomez, D.W. Higinbotham, J.O. Hansen, C. W. de Jager, M. Jones, J. LeRose, W. Melnitchouk, R. Michaels, S. Nanda, B. Reitz, A. Saha, B. Wojtsekhowski
Jefferson Lab, Newport News, Virginia.

W. Korsch
University of Kentucky, Lexington, Kentucky.

J.J. Kelly, C.C. Chang
University of Marylan, College Park, Maryland.

K. Paschke
University of Massachusetts, Amherst, Massachusetts.

W. Bertozzi, O. Gayou, S. Gilad, B. Ma, P. Monaghan, X. Zheng
Massachusetts Institute of Technology, Cambridge, Massachusetts.

P. Ulmer, L. Weinstein
Old Dominion University, Norfolk, Virginia.

F. Benmokhtar, R. Gilman, C. Glashausser, X. Jiang (Co-Spokesperson) [a] ,
G. Kumbartzki, K. McCormick, R. Ransome.

Rutgers University, Piscataway, New Jersey.

F. Butaru, Seonho Choi, Z.-E. Meziani, K. Slifer, P. Solvignon, H. Yan

Temple University, Philadelphia, Pennsylvania.

G. Cates, A. Deur, R. Lindgren, N. Liyanage, B. Norum, K. Wang

University of Virginia, Charlottesville, Virginia.

T. Averett, K. Kramer, V. Sulkosky, X. Zhu

College of William and Mary, Williamsburg, Virginia.

T. Ruan, J. Shen, Z. Yin, Y. Ye

University of Science and Technology of China, Hefei, P.R.China.

J. Yuan, S. Zhou

China Institute of Atomic Energy, Beijing, P.R.China.

J.R.M. Annand, D. Ireland, J.D. Kellie, K. Livingston, R. Kaiser, D. Protopopescu,
G. Rosner, D. Watts.

University of Glasgow, Glasgow, Scotland, United Kingdom.

F. Cusanno, S. Frullani, F. Garibaldi, G. Urciuoli, M. Iodice, R. De Leo, L .La Gamba

INFN Roma–I, INFN Roma–III, INFN Bari and University of Bari, Italy

M. Potokar, S. Širca

Jozef Stefan Institute, and University of Ljubljana, Ljubljana, Slovenia

A. J. Sarty

St. Mary's University, Halifax, Nova Scotia, Canada.

E. Piasetzky

Tel Aviv University, Tel Aviv, Israel

V. Nelyubin

St-Petersburg Nuclear Physics Institute, Gatchina, Leningrad district, 18835, Russia.

[a] Contact person, email: jiang@jlab.org

Abstract: We propose to measure the target single spin asymmetry in the semi-inclusive deep-inelastic $\vec{n}(e, e'\pi^-)X$ reaction with a transversely polarized ^{3}He target. The goal of this experiment is to provide the first measurement on the neutron transversity, complementary to the ongoing COMPASS and HERMES measurements on the proton. This experiment focuses on the valence quark region, $x = 0.19 \sim 0.34$, at $Q^2 = 1.77 \sim 2.73$ GeV^2. This kinematics is comparable to the HERMES measurement. The variation of single spin asymmetry as a function of Collins angle will provide a clear differentiation between the two competing mechanisms–the chiral-even Sivers effect and the chiral-odd Collins effect. This is a crucial step towards the extraction of the quark transversity distributions in semi-inclusive deep-inelastic scattering. The variation of single spin asymmetry relative to x and z will isolate effect of parton distribution from that of fragmentation. Data from this experiment, when combined with proton data from HERMES and COMPASS, will provide powerful constraints on the transversity distributions on both u–quark and d-quark in the valence region. A total of 24 days of beam time at 6 GeV in Hall A is requested.

Contents

1 Introduction

The topic of single spin asymmetry in semi-inclusive deep-inelastic scattering has received much attention in the past two years [1]. This attention was stimulated by the data from HERMES run–I, in which non-vanishing azimuthal asymmetries were reported in pion production on a polarized proton target [2,3]. For the first time, it appears that an observable can be attributed to the effect of the quark transverse spin, and a time-reversal odd quark fragmentation process can be identified. When HERMES finishes taking its transversely polarized proton target data by 2004, information on the u–quark transversity distribution and its T–odd fragmentation function should become available [4]. However, information on the neutron single spin asymmetry will remain unavailable. This experiment is designed to provide the first data on the neutron single spin asymmetry through $\vec{n}(e,e'\pi^-)X$ measurement on a transversely polarized ^{3}He target. At $x = 0.19 \sim 0.34$, $Q^2 = 1.77 \sim 2.73$ GeV^2, comparable to the HERMES kinematics, data from this experiment will be complementary to the HERMES run-II proton data, with which it can be combined to provide powerful constraints on the transversity distributions of both u–quark and d–quark.

2 Physics Motivation

2.1 Transversity distributions of the nucleon

At the leading twist, three fundamental quark distributions provide a complete description of quark momentum and spin in the nucleon [5]. The unpolarized quark distributions are well-known, thanks to the extensive deep-inelastic scattering (DIS) data collected over the last three decades. The longitudinal polarized quark distributions are also reasonably known from the polarized DIS data, and more recently from the semi-inclusive deep-inelastic scattering (SIDIS) data of HERMES and SMC. The third type of distribution, the "transversity distribution", despite strong theoretical and experimental interest, remains practically unknown.

The transversity distribution (h_1^q) can be interpreted as the probability to find a transversely polarized quark in a transversely polarized nucleon [6]. Unlike the unpolarized and longitudinally polarized distributions (f_1^q and g_1^q), which are chiral-even quantities, the transversity distribution has a chiral-odd structure. Due to this chiral-odd nature, the transversity distribution can not be accessed through inclusive DIS processes because an additional chiral-odd object is required.

The transversity distributions have many interesting theoretical aspects, related to general properties of QCD as well as to the structure of the nucleon:

- In the non-relativistic quark model (no spin–orbit interaction), where boosts and rotations commute, the transversity distributions are identical to the longitudinally polarized distributions. Since the quarks inside the nucleon cannot

be non-relativistic, the transversity distributions provide a detailed measure of the relativistic nature of the quarks inside the nucleon.

- The transversity distribution is expected to follow a valence like behavior. Since the transversity of gluons in a nucleon does not exist, the transversity distribution does not mix with gluons in its evolution, and is expected to follow a simple evolution as a flavor non-singlet quantity [7].

- The transversity obeys some important inequalities. The first, $|h_1^q| \leq f_1^q$, follows from its interpretation as a difference of probabilities. The second (Soffer's bound) has its origins in the positivity of helicity amplitudes [8]: $|h_1^q| \leq \frac{1}{2}(f_1^q + g_1^q)$.

- The lowest moment of h_1^q measures a simple local operator analogous to the axial charge, known as the "tensor charge". Unlike its vector and axial equivalents, the tensor charge evolves with Q^2.

2.2 Single-spin azimuthal asymmetry in semi-inclusive pion electroproduction

It has been proposed that the transversity distribution can manifest itself in SIDIS reactions through the Collins effect [9], where the transversity distribution can be probed through a chiral–odd T–odd quark fragmentation function—the Collins function. Indeed, an analysis of $Z^\circ \to 2$ jets decay indicated that the Collins fragmentation function has a sizable magnitude [10]. Recent results on target single spin azimuthal asymmetries in SIDIS reactions from HERMES and SMC [11] offered the first glimpse of possible effects caused by the transversity distribution.

The kinematics and the coordinate definition are illustrated in Fig. 1. We define E′ as the energy of the scattered electron and θ_e is the scattering angle, $\nu = E - E'$ is the energy transfer. The Bjorken-x, which indicates the fractional momentum carried by the struck quark, is defined as: $x = Q^2/(2\nu M_N)$, M_N is the nucleon mass. The momentum of the outgoing pion is p_π and the fraction of the virtual photon energy carried by the pion is: $z = E_\pi/\nu$. W is the invariant mass of the whole hadronic system and W' is the invariant mass of the hadronic system without the detected pion. We have:

$$\begin{aligned} W^2 &= M_N^2 + Q^2(\frac{1}{x} - 1), \\ W'^2 &= (M_N + \nu - E_\pi)^2 - |\vec{q} - \vec{p}_\pi|^2. \end{aligned} \tag{1}$$

The pion transverse momentum relative to $\vec{q}$ is labeled as $P_{h\perp}$. At the leading order, when h is a spin zero particle, the spin-dependent cross section[12,13,14] is:

$$d^6\sigma^{LO} = \frac{d\sigma^{\ell+N\to\ell'+h+X}}{dxdyd\phi^\ell dzd^2\boldsymbol{P}_{h\perp}} = \frac{4\pi\alpha^2\, s\, x}{Q^4} \times$$

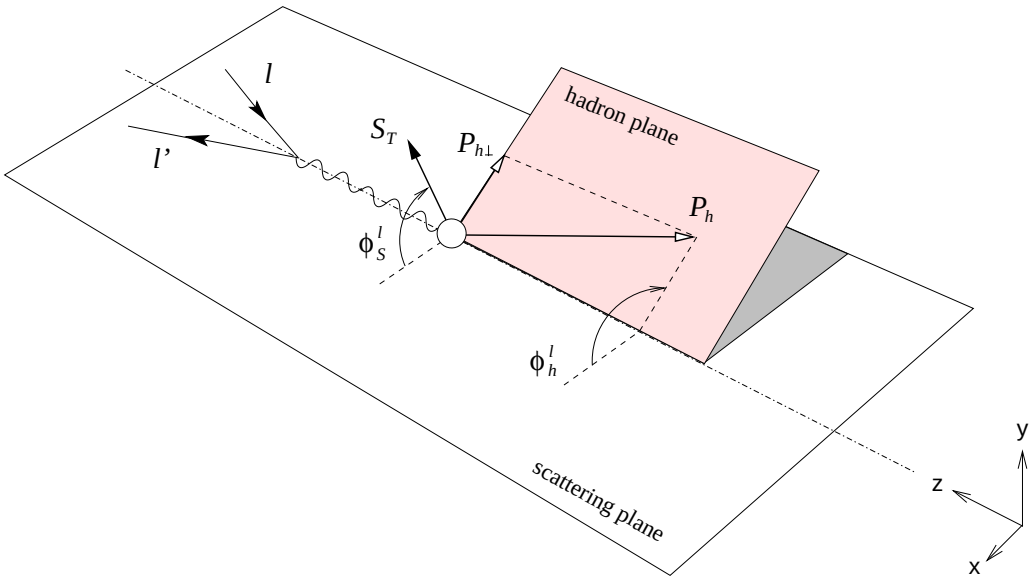

Figure 1: The definition of the coordinates.

$$
\begin{aligned}
&\Big\{\Big[1+(1-y)^2\Big]\ \sum_{q,\bar{q}} e_q^2\, f_1^q(x) D_1^q(z, \boldsymbol{P}_{h\perp}^2) \\
&+(1-y)\frac{P_{h\perp}^2}{4z^2 M_N\, M_h}\ \cos(2\phi_h^\ell) \sum_{q,\bar{q}} e_q^2\, h_1^{\perp(1)q}(x) H_1^{\perp q}(z, \boldsymbol{P}_{h\perp}^2) \\
&-|\boldsymbol{S}_L|\,(1-y)\frac{P_{h\perp}^2}{4z^2 M_N\, M_h}\ \sin(2\phi_h^\ell) \sum_{q,\bar{q}} e_q^2\, h_{1L}^{\perp(1)q}(x) H_1^{\perp q}(z, \boldsymbol{P}_{h\perp}^2) \\
&+|\boldsymbol{S}_T|\,(1-y)\frac{P_{h\perp}}{zM_h}\ \sin(\phi_h^\ell + \phi_S^\ell) \sum_{q,\bar{q}} e_q^2\, h_1^q(x) H_1^{\perp q}(z, \boldsymbol{P}_{h\perp}^2) \\
&+|\boldsymbol{S}_T|\ \left(1-y+\frac{1}{2}\,y^2\right)\frac{P_{h\perp}}{zM_N}\ \sin(\phi_h^\ell - \phi_S^\ell) \sum_{q,\bar{q}} e_q^2\, f_{1T}^{\perp(1)q}(x) D_1^q(z, \boldsymbol{P}_{h\perp}^2) \\
&+|\boldsymbol{S}_T|\,(1-y)\frac{P_{h\perp}^3}{6z^3 M_N^2\, M_h}\ \sin(3\phi_h^\ell - \phi_S^\ell) \sum_{q,\bar{q}} e_q^2\, h_{1T}^{\perp(2)q}(x) H_1^{\perp q}(z, \boldsymbol{P}_{h\perp}^2) \\
&+\lambda_e\,|\boldsymbol{S}_L|\, y\,(1-\frac{1}{2}\,y) \sum_{q,\bar{q}} e_q^2\, g_1^q(x) D_1^q(z, \boldsymbol{P}_{h\perp}^2) \\
&+\lambda_e\,|\boldsymbol{S}_T|\, y\,(1-\frac{1}{2}\,y)\frac{P_{h\perp}}{zM_N}\ \cos(\phi_h^\ell - \phi_S^\ell) \sum_{q,\bar{q}} e_q^2\, g_{1T}^{(1)q}(x) D_1^q(z, \boldsymbol{P}_{h\perp}^2)\Big\}. \qquad (2)
\end{aligned}
$$

where $|\boldsymbol{S}_L|$ and $|\boldsymbol{S}_T|$ are the longitudinal and transverse spin component, λ_e is the electron helicity. Azimuthal angles are defined relative to the lepton plane, e.g. $\phi_h^\ell = \phi_h - \phi^\ell$ is the angle between the hadron plane ($\vec{P}_h \wedge \vec{q}$) and the lepton plane. $\phi_S^\ell = \phi_S - \phi^\ell$ is the angle between the $\vec{S} \wedge \vec{q}$ plane and the lepton plane.

Fig. 2 gives a pictorial representation of the distribution functions. The distri-

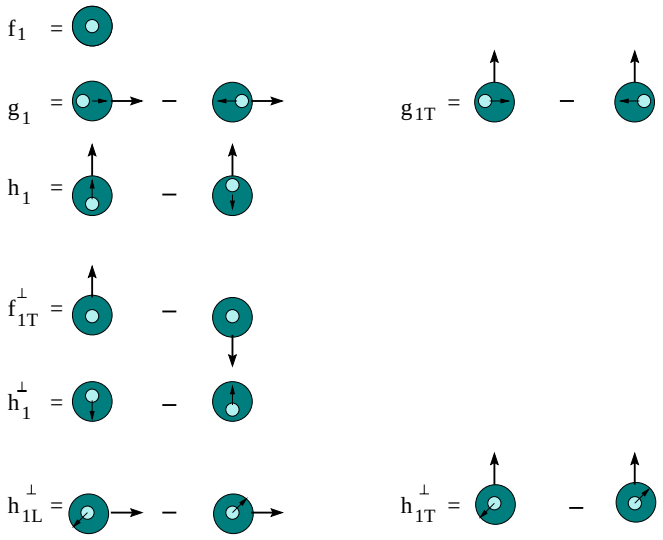

Figure 2: A pictorical representation of the distribution functions [?]. Three functions, $f_1^q(x)$, $g_1^q(x)$ and $h_1^q(x)$ survive the integration of quark $\boldsymbol{p}_T$.

bution $f_1^q(x)$ is the probability of finding an unpolarized quark in an unpolarized nucleon; $g_1^q(x)$ is for a longitudinally polarized quark in a longitudinally polarized nucleon and $h_1^q(x)$ is for a transversely polarized quark in a transversely polarized nucleon. These three functions survive the integration of intrinsic quark transverse momentum $\boldsymbol{p}_T$ in the initial nucleon. The corresponding $\boldsymbol{p}_T$ dependent distributions are $f_{1T}^{\perp q}$, $g_{1T}^{\perp q}$, $h_1^{\perp q}$, $h_{1L}^{\perp q}$ and $h_{1T}^{\perp q}$. They only survive the $\boldsymbol{p}_T$ integration after weighting with $(\boldsymbol{p}_T^2/2M_N^2)^n$. Such weighting is indicated by a superscript (n) in Eq. 2.

With unpolarized beam and a transversly polarized target, three terms in Eq. 2 contribute to the single target-spin asymmetry. The $\sin(\phi_h^\ell + \phi_S^\ell)$ term is the Collins effect, which involves the chiral-odd transversity distribution $h_1^a(x)$ and the chiral-odd and T-odd Collins fragmentation function $H_1^{\perp a}$. The $\sin(\phi_h^\ell - \phi_S^\ell)$ term is the Sivers effect, which involves the chiral-even T-odd Sivers distribution function $f_{1T}^{\perp a}(x)$ and the regular fragmentation function D_1^a. The Sivers function is non-vanishing at the leading twist [17,18], and is due to the asymmetric distribution of quark transverse momentum in a nucleon. The $\sin(3\phi_h^\ell - \phi_S^\ell)$ term, compared to the Collins term, contains an extra factor of $\frac{1}{6}(P_{h\perp}/zM_N)^2$ which amounts to only 0.03–0.13 in this experiment. In addition, one expects that $h_{1T}^{\perp(2)a}(x) \ll h_1^a(x)$ due to quark transverse momentum weighting. Therefore, we assume contribution from the $\sin(3\phi_h^\ell - \phi_S^\ell)$ term is negligible. Similarly, the $\cos(2\phi_h^l)$ term of the unpolarized cross section can be neglected in the asymmetry expression. For a 100% polarized nucleon, the transverse momentum dependent single target-spin asymmetry is:

$$\begin{aligned} A_T(x, z, \boldsymbol{P}_{h\perp}^2) &= (A_T)_{Collins} + (A_T)_{Sivers} \\ &= \frac{1-y}{1-y+\frac{1}{2}y^2} \cdot \frac{P_{h\perp}}{zM_h} \sin(\phi_h^\ell + \phi_S^\ell) \cdot \frac{\sum_{q,\bar{q}} e_q^2\, h_1^q(x) H_1^{\perp q}(z, \boldsymbol{P}_{h\perp}^2)}{\sum_{q,\bar{q}} e_q^2\, f_1^q(x) D_1^q(z, \boldsymbol{P}_{h\perp}^2)} \end{aligned}$$

$$+\frac{P_{h\perp}}{zM_N}\,\sin(\phi_h^\ell-\phi_S^\ell)\cdot\frac{\sum_{q,\bar{q}}e_q^2\,f_{1T}^{\perp(1)q}(x)D_1^q(z,\boldsymbol{P}_{h\perp}^2)}{\sum_{q,\bar{q}}e_q^2\,f_1^q(x)D_1^q(z,\boldsymbol{P}_{h\perp}^2)} \tag{3}$$

2.3 Data from HERMES and SMC and interpretations

The HERMES collaboration has recently reported[2,3] the single spin azimuthal asymmetries for charged and neutral pion electroproduction based on a SIDIS data sample of $\langle Q^2\rangle = 2.5$ GeV^2. Using an unpolarized positron beam on a longitudinally polarized proton target (such that $\phi_S^l = 0$), the cross section was found to have a $\sin\phi_h^l$ dependence in both π^+ and π^0 production as shown in Fig. 3. This single spin

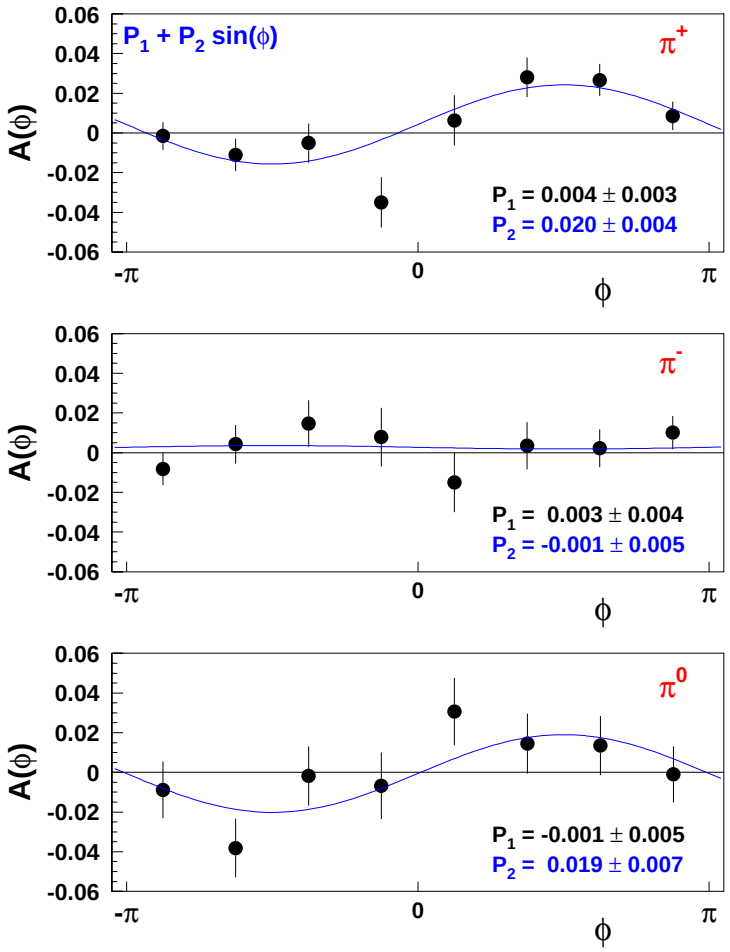

Figure 3: Analyzing power as a function of $\phi = \phi_h^l$ from HERMES [2,3] proton target measurements. Solid lines indicate fits of $P_1 + P_2\sin(\phi_h^l)$.

asymmetry can be expressed as the analyzing power in the $\sin\phi_h^l$ moment, and the result is shown in Fig. 4 as a function of pion fractional energy z, Bjorken x, and the pion transverse momentum $P_\perp$. The $\sin\phi_h^l$ moment for an unpolarized (U) positron

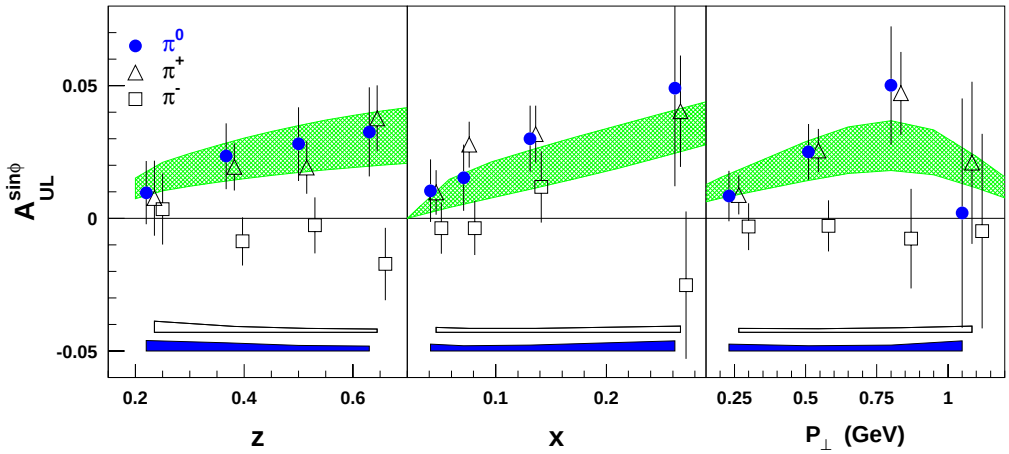

Figure 4: Analyzing power in the $\sin\phi_h^l$ moment from HERMES [2,3] proton target measurements. Solid bands that fit the data assume that the transversity distributions range from $h_1 = g_1$ to $h_1 = (f_1 + g_1)/2$. Error bars include the statistical uncertainty only. The bands at the bottom of the panels represent the systematic uncertainties.

scattered off a longitudinally (L) polarized target contains two main contributions

$$\langle sin\phi_h^l \rangle \propto 4S_L \frac{M}{Q}(2-y)\sqrt{1-y}\sum_{q,\bar{q}} e_q^2 \left(h_L^q(x) H_1^{\perp q}(z) - h_{1L}^{\perp q(1)}(x)\tilde{H}(z) \right)$$
$$-2S_T(1-y)\sum_{q,\bar{q}} e_q^2 h_1^q(x) H_1^{\perp q}(z). \qquad (4)$$

For the HERMES experiment with a longitudinally polarized target, the transverse component is nonzero with a mean value of $S_T \approx 0.15$. The observed azimuthal asymmetry could be a combined effect of h_1^q–the twist-2 transversity distribution, and h_L^q–the twist-3 distribution function in the longitudinally polarized nucleon [15]. Figure 4 shows that a model calculation [15,16] reproduces the z, x, and $p_\perp$ dependences of the π° asymmetry. The striking difference between the π^+ and π^- analyzing power suggests that the u-quark dominates the proton asymmetry.

If the azimuthal asymmetry observed by HERMES is indeed caused by the h_1^q transversity distribution, a much larger asymmetry is expected for a transversely polarized target. An earlier SMC measurement on a transversely polarized proton target, as shown in Fig. 5, had limited statistics and was inconclusive [11]. The HERMES run–II plans to have a dedicated two-year transversely polarized proton target run to measure the shape of $h_1^u(x)$ (and $H_1^u(z)$).

Complicating the situation, it was recently found that a chiral-even mechanism previously considered forbidden (the Sivers effect), is actually allowed in SIDIS, adding contributions in competition with the Collins effect. Using a QCD motivated quark-diquark model, Brodsky *et al.* [17] demonstrated that the final state interactions from gluon exchange between the outgoing quark and the target spectator leads to a sizable single spin asymmetry. This quark final state interaction is interpreted [18] as giving rise to the chiral-even T-odd Sivers function [19]. It was further demonstrated [20]

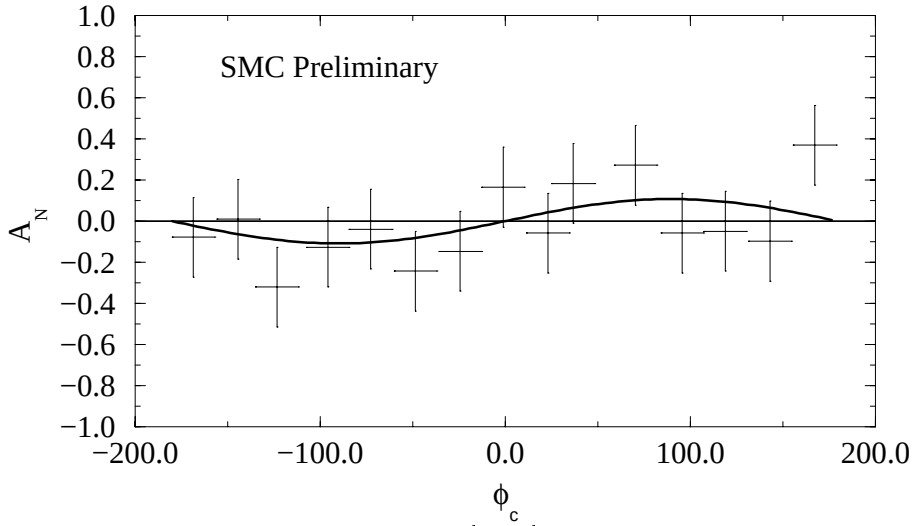

Figure 5: Analyzing power as a function of $\phi_c = \phi_h^l + \phi_S^l$ from SMC [11] on a transversely polarized proton target.

that the quark final-state interactions can be fully accounted for in the light-cone approach. Both the Collins effect and the Sivers effect can contribute to the observed single spin asymmetry.

Fortunately, in a measurement involving a transversely polarized target, the two competing mechanisms can be distinguished by observing single spin asymmetry as a function of the Collins angle. The Collins effect, which involves transversity distributions and chiral-odd fragmentation functions, contributes a $\sin(\phi_h^l + \phi_S^l)$ dependence to the cross section. The Sivers effect, which involves chiral-even T-odd distribution functions and chiral-even fragmentation functions, contributes a $\sin(\phi_h^l - \phi_S^l)$ dependence. In addition, the two competing contributions have different kinematic dependences. The Collins effect depends on a kinematic factor of $(1-y)/(1-y+\frac{1}{2}y^2)$ and is strongly correlated with z, but the Sivers effect is independent of y and not strongly correlated with z, where $y = \nu/E$ and $z = E_\pi/\nu$. Therefore, with a transversely polarized target and a broad coverage in Collins angles, y and z, such as in HERMES run–II and in this experiment, differentiation between the Collins effect and the Sivers effect becomes possible.

2.4 Opportunity for a transversity measurement at Jlab on a transversely polarized ^{3}He target

In order to confront theoretical predictions on the transversity distribution and on transverse single spin asymmetry, precise SIDIS data on both the proton and the neutron covering a wide range of kinematics is required. The experimental situation is expected to be significantly improved in the near future with new data currently being collected at COMPASS and HERMES. If the Collins effect turns out to dominate the single spin asymmetry, the transversity distribution of the u–quark is expected to be extracted with reasonable accuracy [4]. A transversely polarized

deuteron target run has also been discussed[4] at HERMES to access the transversity distribution of $h_1^u + h_1^d$, however, it is not clear if such a run can fit into the HERA schedule in the near future. We point out here that although HERMES has the advantage of a 27.5 GeV beam, its forward angle geometry and the 10^{32} cm^{-2}s^{-1} polarized target luminosity limit its SIDIS event sample to an average Q^2 of 2.5 GeV^2. A similar Q^2 range for $x = 0.19 \sim 0.34$ can be accessed at the Jefferson Lab Hall A with a 6 GeV electron beam. This is due to the fact that Hall A operates at a much higher luminosity, 10^{36} cm^{-2}s^{-1} for polarized ^{3}He, which allows SIDIS events to be sampled at a much larger scattering angle. Figure 6 shows the expected statistical precision of this experiment on $\vec{n}(e, e'\pi^-)X$ single spin asymmetry together with the projected precision of HERMES run–II of the $\vec{p}(e, e'\pi^+)X$ reaction.

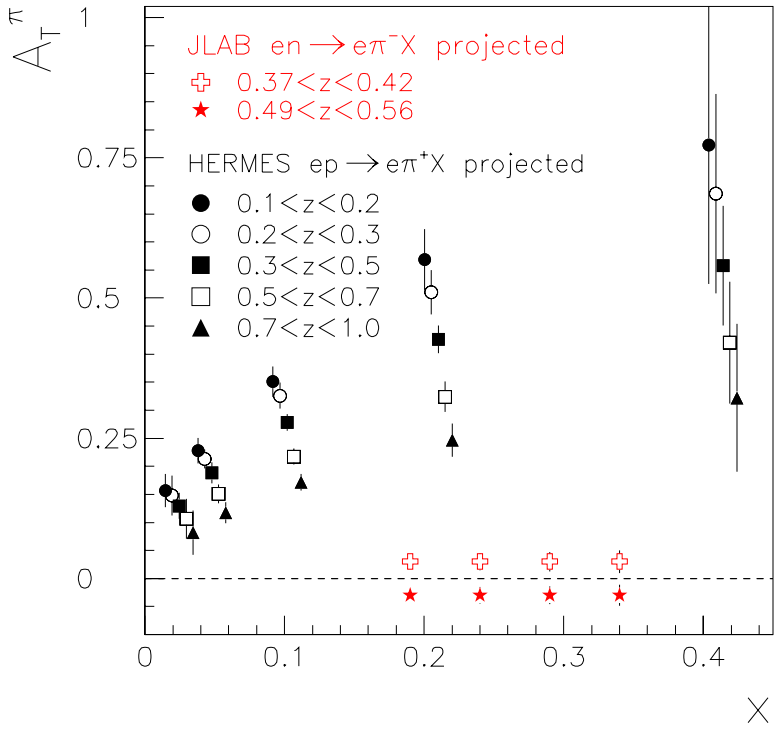

Figure 6: Expected statistical precision of this experiment in comparison with HERMES run-II projected precision on a proton target [4]. The uncertainties from this experiment are generally smaller than the plotted symbols.

The transverse single spin asymmetry measurements at both HERMES and COMPASS are using polarized proton or deuteron targets, of which the u–quark is the dominating flavor due to charge weighting. In contrast, this experiment plans to measure the single spin asymmetry of the $\vec{n}(e, e'\pi^-)X$ reaction on a transversely polarized ^{3}He target. Since a polarized ^{3}He target is effectively a polarized neutron target, contributions from both u–quark and d–quark are expected to be comparable. At a Q^2 similar to the HERMES measurement, this experiment will, for the first time, provide precision data on neutron single spin asymmetry, complementary to the proton data from HERMES run–II. Since the same fragmentation functions

are involved in both cases, this experiment, when combined with the proton data from HERMES, will provide powerful constraints on the transversity distributions in the valence region.

2.5 Model predictions of transverse target single spin asymmetry

From Eq. 3, assuming only the Collins effect contributes, the azimuthal asymmetry A_T is [21]:

$$A_T(x, z, \boldsymbol{P}_{h\perp}^2) = \frac{1-y}{1-y+\frac{1}{2}y^2} \cdot \left(\frac{|\boldsymbol{P}_\perp|}{zM_h}\right) \cdot \frac{\sum_q h_1^q(x) H_1^{\perp q}(z, \boldsymbol{P}_\perp^2)}{\sum_q f_1^q(x) D_1^q(z, \boldsymbol{P}_\perp^2)}, \tag{5}$$

Omitting the explicit Q^2 notation, the transverse momentum dependent fragmentation function $D_1^q(z, \boldsymbol{P}_\perp^2)$ relates to the normal fragmentation function through the integration of the scattered quark transverse momentum $\boldsymbol{k}_T = \boldsymbol{P}_\perp/z$:

$$z^2 \int d^2\mathbf{k_T} D_1^q(z, \boldsymbol{P}_\perp^2) \equiv D_1^q(z). \tag{6}$$

Collins suggested [18] that the analyzing power in transversely polarized quark fragmentation follow:

$$A_C(z, k_T) \equiv \frac{|\boldsymbol{k}_T| H_1^{\perp q}(z, \boldsymbol{P}_\perp^2)}{M_h D_1^q(z, \boldsymbol{P}_\perp^2)} = \frac{M_C |\boldsymbol{k}_T|}{M_C^2 + |\boldsymbol{k}_T^2|}, \tag{7}$$

with $M_C = 0.3 \sim 1.0$ GeV. HERMES analysis takes $M_C = 0.7$ GeV as a rough guess [4], which we will follow in our numerical estimates. The transverse momentum dependence of $D_1^q(z, \boldsymbol{P}_\perp^2)$ is assumed to have a Gaussian type shape:

$$D_1^q(z, \boldsymbol{P}_\perp^2) = D_1^q(z) \cdot \frac{R^2}{\pi z^2} exp(-R^2 \boldsymbol{P}_\perp^2/z^2), \tag{8}$$

with $R^2 = z^2/b^2$, and b^2 is the mean-square momentum the hadron acquires in the quark fragmentation process with $b^2 = 0.25$ (GeV/c)^2 according to HERMES [22].

The predictions [21] of A_T from a quark diquark model and a PQCD based analysis are shown in Fig. 7 for π^+ on a proton and π^- on a neutron. The calculation in Fig. 7 has been integrated over z and the pion transverse momentum $P_\perp$ to demonstrate the x-dependence at the HERMES kinematics of $Q^2 = 2.5$ GeV^2. A sizable asymmetry on the neutron is expected in the valence quark region. In this experiment we will focus on the valance quark region ($x = 0.19 \sim 0.34$) and measure $\vec{n}(e, e'\pi^-)X$ reaction with a transversely polarized ^{3}He target.

3 The Proposed Measurement

3.1 Overview

We plan to study the target single spin asymmetry (SSA) in the semi-inclusive deep-inelastic $\vec{n}(e, e'\pi^-)X$ reaction on a polarized ^{3}He target in Hall A with a 6

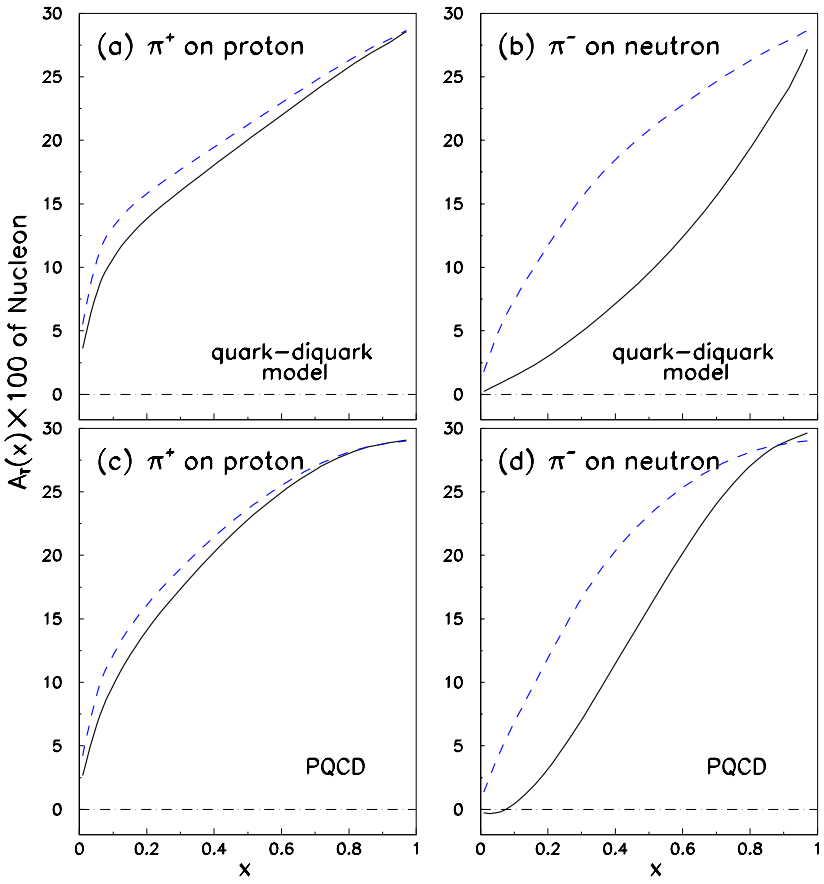

Figure 7: Transverse single-spin asymmetry for the proton target [21]. The upper row corresponds to predictions of quark diquark model, and the lower row corresponding predictions of the PQCD based analysis. The solid curves are the calculated results with both favored and unfavored fragmentation, the dashed curves are the results with only favored fragmentation.

GeV beam. The average beam current will be $\approx 15\ \mu$A. Although a polarized beam is not required to perform the SSA measurements, we request an 80% polarized electron beam for parasitic double-spin asymmetry measurements. Analysis of SSA will sum over the two beam helicities. The experiment will use the Hall A left side high resolution spectrometer (HRS_L) situated at 16° as the hadron arm, and use the BigBite spectrometer at 30° beam-right as the electron arm. The BigBite detector configuration will be exactly the same as in the approved Hall A G_E^n experiment [23] (E02013). The drift distance to the BigBite dipole magnet will be 1.50 meter, instead of the 1.10 meter drift in E02013. The Hall A high luminosity polarized ^{3}He target will be used with a 40 cm long cell. The Helmholtz coils and laser optics need to be modified to provide a target polarization along two specific orientations: the vertical direction and 45° off the vertical direction. The experimental arrangement is illustrated in Fig. 8 and a close-up view near the pivot is shown in Fig. 9.

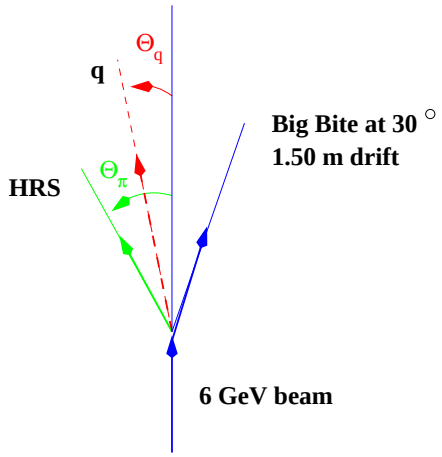

Figure 8: Experiment arrangement, target polarization is in the plane that is perpendicular to the plane of $\vec{q} \wedge (\vec{q} \times \vec{p}_{\pi})$.

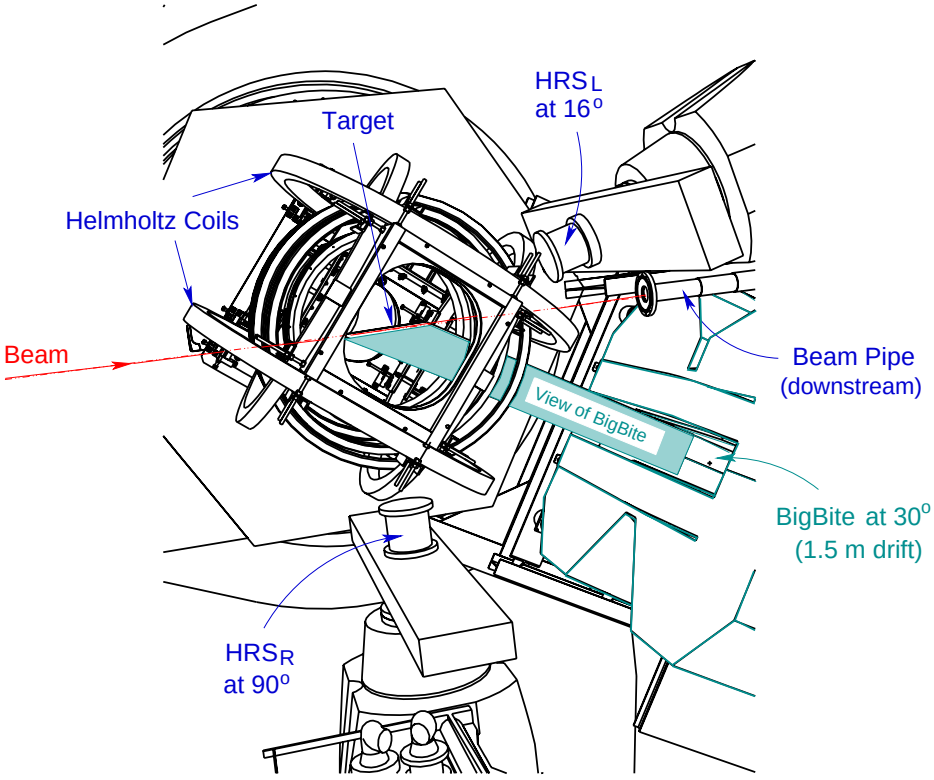

Figure 9: A top view near the pivot. The left HRS is shown at 16°, the BigBite dipole magnet is shown at 30° beam right and at a 1.5 meter drift distance. The right HRS is at 90° as a luminosity monitor. The target coils are arranged to avoid interference with the beam line and the spectrometers.

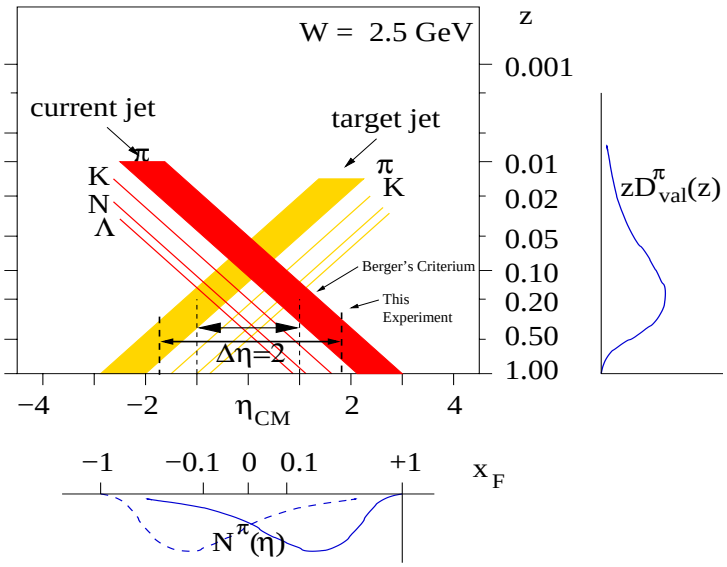

Figure 10: The center-of-mass rapidity gap [24] for $W = 2.5$ GeV (the highest x-bin), above $z = 0.37$ the current and target fragmentation regimes are separated by $\Delta\eta_{CM} = 3.5$. A typical fragmentation function is shown on the side panel with $z = E_\pi/\nu$ and $x_F = p_L^{\pi\star}/|\vec{q}|$.

3.2 The choice of kinematics

We chose to cover the highest possible W with a 6 GeV beam, $2.49 < W < 2.88$ GeV, corresponds to $0.19 < x < 0.34$ and $1.77 < Q^2 < 2.73$ (GeV/c)^2. We also chose to detect the leading fragmentation pion which carries $z = 0.37 \sim 0.56$ of the energy transfer to favor the current fragmentation. In the two-dimensional plot [24] of z vs the center of mass rapidity η_{CM}, where $\eta_{CM} = \frac{1}{2} ln \frac{E+P_L^\star}{E-P_L^\star}$ defined in the center of mass frame, as shown in Fig. 10 for the worst case of the $x = 0.34$ bin with $W = 2.5$ GeV, the rapidity gap between the two fragmentation regimes is at least $\Delta\eta_{CM} = 3.5$ when $z > 0.37$ is required. This requirement is well above the regularly used Berger's Criterion of $\Delta\eta_{CM} = 2.0$ for separation of current and target fragmentation [25].

The value of W' is also chosen to be as high as possible (1.75∼2.29 GeV) to avoid contributions from resonance structures. The central kinematic values for each x-bin are listed in Table 1. Because of the large momentum bite of the BigBite spectrometer, only one BigBite setting is needed to cover all the kinematics listed in Table 1. Two hadron arm momentum settings, $p_\pi = 1.8$ and 2.4 GeV/c, will be taken. The corresponding values of W', z and $P_\perp$ for each x-bin are listed in Table 1.

3.3 The phase space and Collins angle coverage

The phase space coverage is obtained from a detailed Monte Carlo simulation which includes realistic spectrometer models as well as target and detector geometry. The

Table 1: Nominal kinematics for beam energy of $E = 6.0$ GeV. One BigBite setting will cover all the kinematics listed. Two HRS_L momentum settings will be taken. E′ and θ_e are the electron arm momentum and angle. Single electron rates for each x-bin of $\Delta x = 0.05$ are listed for 15 μA beam. θ_q indicates the direction of $\vec{q}$. The hadron arm angle is fixed at 16°.

E′ GeV	θ_e deg.	$\langle x \rangle$	W GeV	Q^2 GeV^2	θ_q deg.	$\mathrm{Rate}_{(e,e')}$ Hz	p_π GeV/c	z	$P_\perp$ GeV/c	W' GeV
1.10	30.0	0.19	2.88	1.77	6.22	185		$\theta_{HRS} = 16.0°$		
							1.80	0.37	0.31	2.29
							2.40	0.49	0.41	2.07
1.30	30.0	0.24	2.76	2.09	7.60	151		$\theta_{HRS} = 16.0°$		
							1.80	0.38	0.26	2.19
							2.40	0.51	0.35	1.97
1.50	30.0	0.29	2.63	2.41	9.06	121		$\theta_{HRS} = 16.0°$		
							1.80	0.40	0.22	2.08
							2.40	0.53	0.29	1.86
1.70	30.0	0.34	2.49	2.73	10.63	96		$\theta_{HRS} = 16.0°$		
							1.80	0.42	0.17	1.96
							2.40	0.56	0.22	1.75

coverage in the (Q^2, x) and (W, x) planes is shown in Fig. 11, and the coverage in the (W', x) and $(P_\perp, x)$ planes is shown in Fig. 12, color coded for each x-bin.

The angular coverage of ϕ_h^l and ϕ_S^l is shown in Fig. 13. The coverage of ϕ_h^l is ±53° for the x=0.19 bin, and ±73° for the x=0.34 bin. This large ϕ_h^l range is due to the fact that the pions are detected close to the $\vec{q}$ direction. The coverage of ϕ_S^l is ±27° and is due to the large vertical acceptance (±240 mrad) of the BigBite. Overall, the coverage of $\phi_h^l \pm \phi_S^l$ is ±80° to ±100° for a given target spin direction ($\vec{S}_T$). Two sets of target spin orientations will be taken at the $P_{HRS} = 1.8$ GeV/c setting, with $\langle \phi_S^l \rangle = \pm 90°$, 135° and −45°. At the $P_{HRS} = 2.4$ GeV/c setting, we will only take $\langle \phi_S^l \rangle = \pm 90°$.

3.4 The electron arm spectrometer BigBite.

The BigBite spectrometer will be located at 30° and at a drift distance of 1.50 meter, instead of the 1.1 meter drift in E02013. The BigBite detector package will be exactly the same as in E02013. Three sets of MWDC chambers will be used to provide tracking information followed by two planes of scintillators (24 pieces each plane) to provide trigger and timing information. A preshower and shower lead glass array at the end will provide particle ID for the electrons. The BigBite dipole magnet will be set at the full current with $|\vec{B}| = 1.2$ T. Charged particles with momentum less than 0.2 GeV/c will be bent away as shown in Fig. 14.

The BigBite collaboration has decided to build three sets of horizontal drift cham-

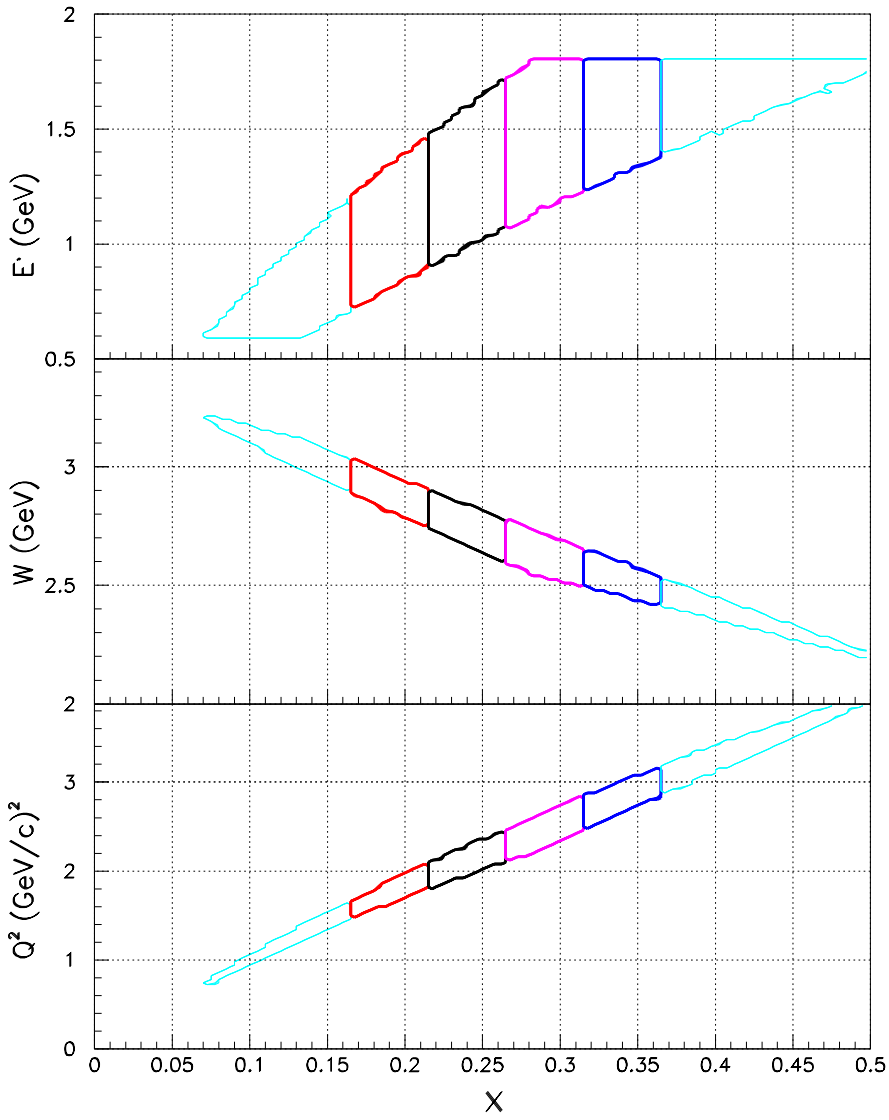

Figure 11: Available phase space in the (Q^2, x) and (W, x) planes with each x-bin in different colors. A cut off of $E' < 1.8$ GeV has been applied, assuming good track and momentum reconstruction in BigBite. The kinematic coverage is wider than the nominal values listed in Table 1. Lower x-region and higher x-region are plotted as light colored contours.

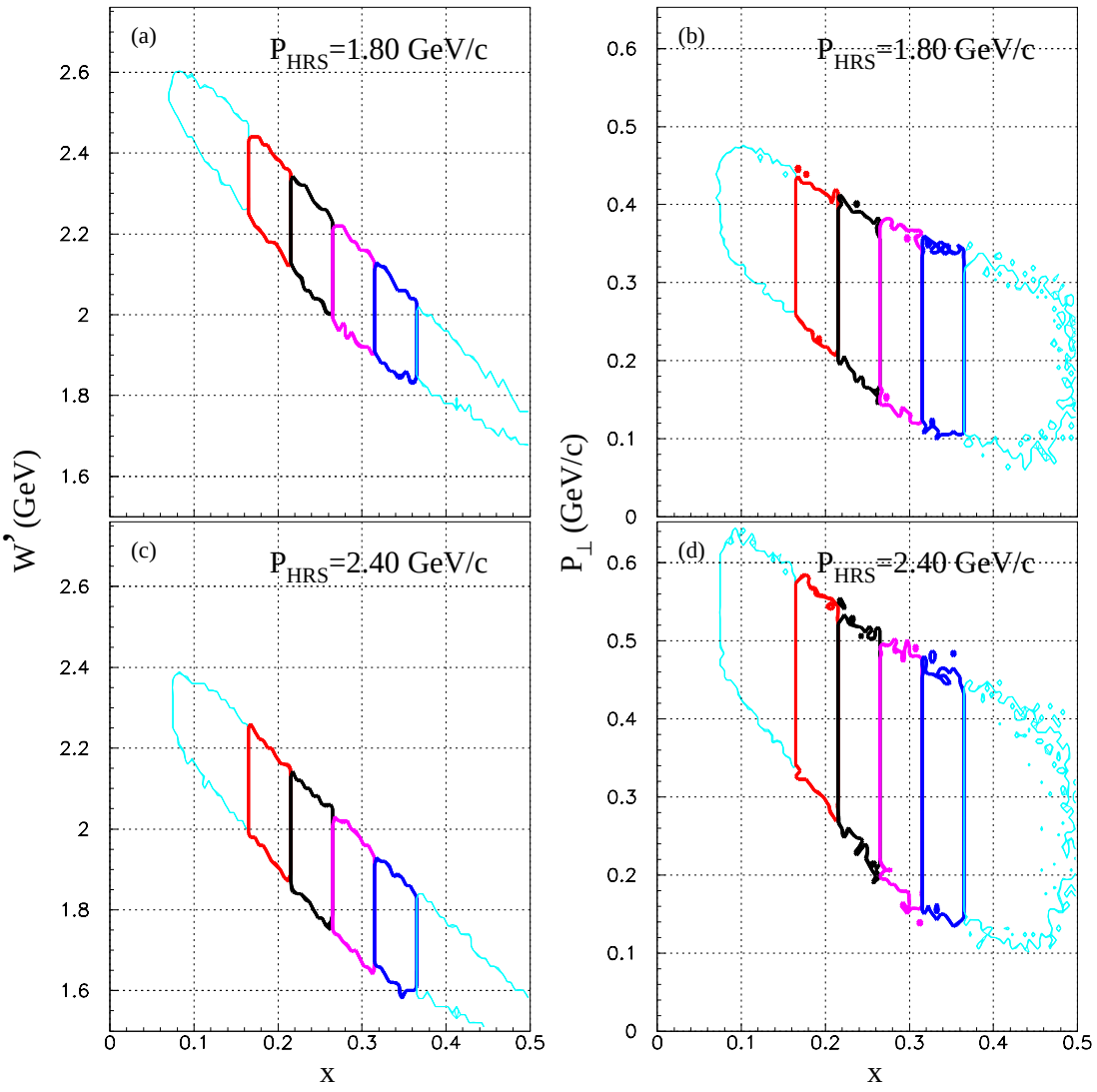

Figure 12: Same as in Fig. 11, phase space coverage in (W', x) and $(P_\perp, x)$ planes. Lower x-region and higher x-region are plotted as light colored contours.

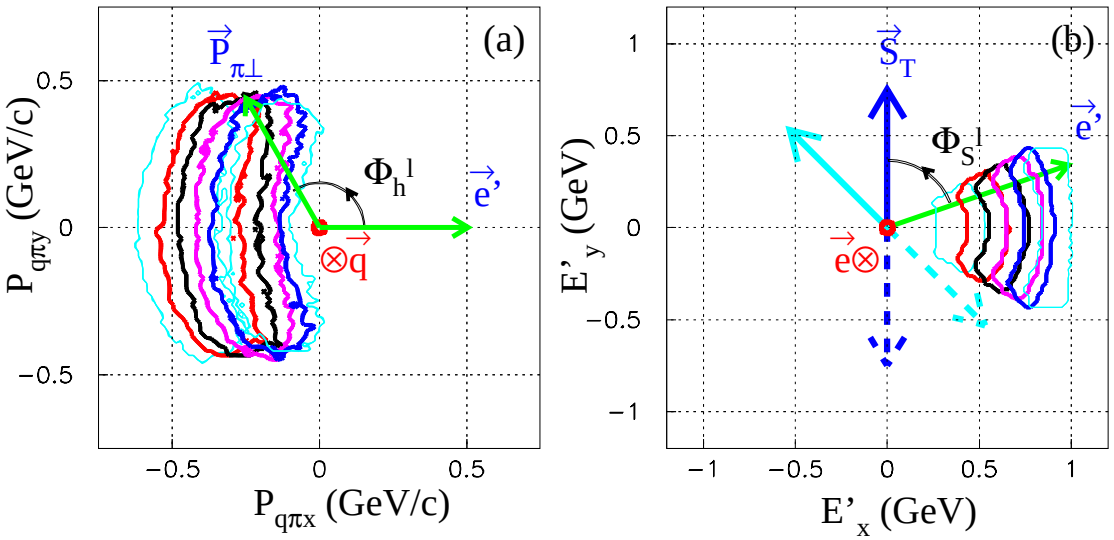

Figure 13: Color coded the same way as in Fig. 11, angular coverage of ϕ_h^l and ϕ_S^l are shown for each x-bin. In (a), viewed along $\vec{q}$, while the scattered electron defines the x-direction, the two components ($P_{q\pi x}$ and $P_{q\pi y}$) of $\vec{P}_{\pi\perp}$ are plotted, showing the range of ϕ_h^l. In (b), viewed along the beam, the two components (E'_x and E'_y) of the scattered electron are plotted, showing the range of ϕ_S^l. Two sets of target spin orientations ($\vec{S}_T$) are shown in (b).

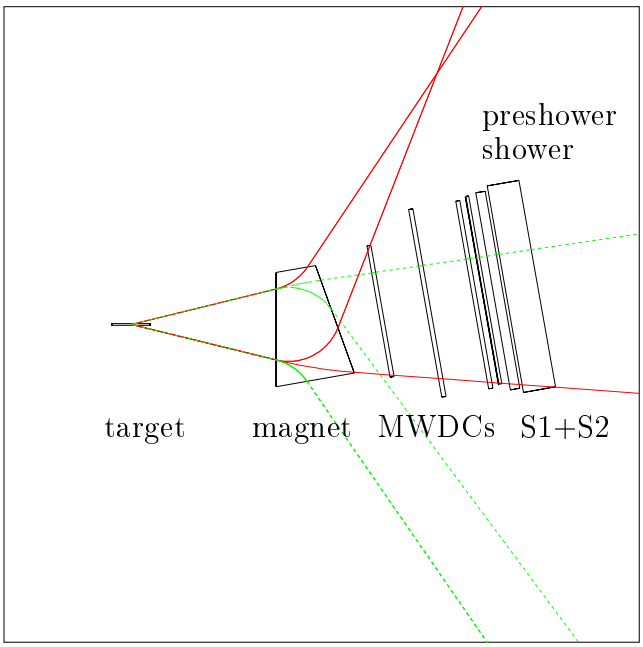

Figure 14: Typical charged particle trajectories through the BigBite spectrometer and its detector package. Particles with $p = 0.2$ and 1.8 GeV/c are shown starting from vertical angles of $\theta_t = \pm 240$ mrad. The upward bending tracks are negatively charged particles, and the downward bending tracks are positively charged particles. The location of wire chambers, trigger scintillator planes, preshower and shower lead glass arrays are also indicated.

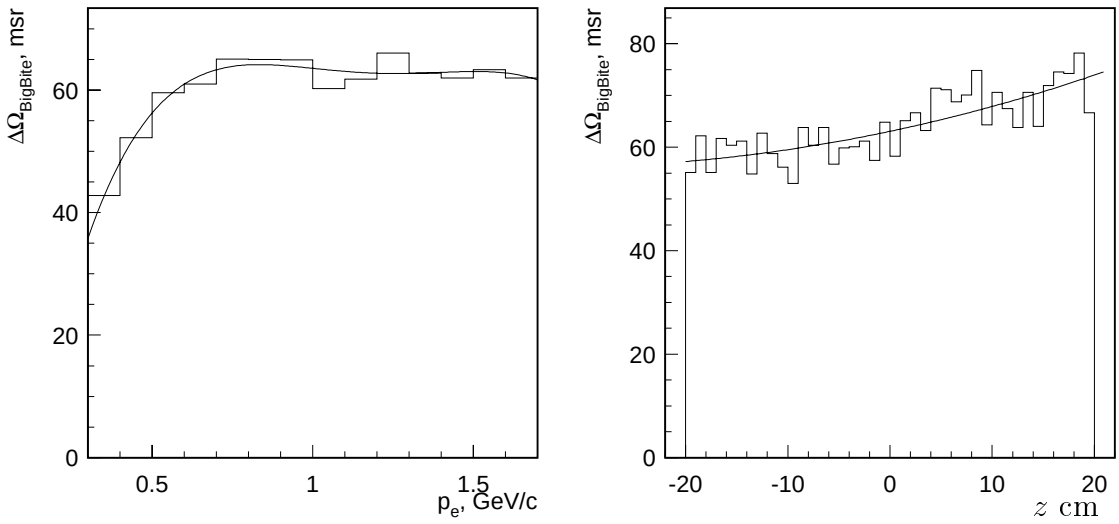

Figure 15: BigBite acceptance as a function of particle momentum (left) and as a function of interaction point (right).

bers, each has U-U′, V-V′ and X-X′ planes. The sense wire separation is 2.0 cm, corresponds to a drift cell size of 1.0 cm and a maximum drift time of 100 ns. A GEANT Monte Carlo simulation [23] shown that with a typical chamber resolution of 200 μm, the momentum resolution ($\delta p/p$) is $\approx 2\%$. The angular resolution is 3.0 mrad in each direction, causing a few MeV uncertainty in $P_\perp$ reconstruction. The vertex resolution will be better than 2.0 cm along the beam. Since this experiment does not seek to resolve any structure in the final states, and the SIDIS events will be grouped in rather large x-bins, the designed momentum and angular resolution of E02013 will be adequate for this experiment.

The electron's particle ID will be provided by a set of preshower and shower detectors. The preshower blocks are made of TF-5 lead glass, $10 \times 10 \times 37$ cm^3 each, covering an active area of 210×74 cm^2, with 10 cm (3 r.l.) along the particle's direction. The total absorption shower blocks are made of TF-2 lead glass, $8.5 \times 8.5 \times 34$ cm^3 each, covering an active area of 221×85 cm^2, with 34 cm (13 r.l.) along the particle's direction. The total depth of lead glass is enough to contain electron showers with energies up to 10 GeV, with an energy resolution of $8.0\%/\sqrt{E}$. A typical pion rejection factor of 100:1 is expected.

The BigBite acceptance as functions of particle momentum and interaction point are shown in Fig. 15. An average solid angle of 64 msr is expected, with the vertical angle $\Delta\theta_t = \pm 240$ mrad ($\pm 13.7^\circ$) and the horizontal angle $\Delta\phi_t = \pm 67$ mrad ($\pm 3.8^\circ$).

Single particle background and track reconstruction in BigBite

The background rates in the BigBite detectors are calculated using the Monte Carlo simulation code GDINR [26]. For particles with momentum above 200 MeV/c, the integrated electron rate is less than 100 kHz, the π^- rate is less than 150 kHz. The positron rate is less than 1 kHz, the π^+ rate is less than 300 kHz. The majority of the charge particle background comes from protons with $p > 200$ MeV/c ($T_p > 21$ MeV). Such proton's rate is 3 MHz, comparable to the situation of E02013, and can be tolerated by the drift chambers.

The low energy photon background in the BigBite is the major concern of this experiment. According to the Monte Carlo, total photon rate could reach 50$\sim$100 MHz, similar to the situation of E02013. Since the maximum drift time in MWDC is 100 ns, the average multiplicity on each plane could reach 5$\sim$ 10 hits per trigger. This relatively high level of chamber activity could cause a large number of candidate tracks for a single arm experiment, or an $(e, e'n)$ type measurement [27], such as in E02013. In a coincidence measurement, however, in which the trigger involves the timing coincidence of two charged particles from two spectrometers, high resolution vertex information from a long target helps in reducing the tracking ambiguity in the BigBite [27], especially when the HRS_L arm is clean. For the BigBite tracking, in the transverse direction, a straight line between the HRS_L reconstructed vertex and the center of shower at the calorimeter serves as the starting point of track reconstruction. In the dispersion direction, the location of shower also helps in track selection. Furthermore, the reconstructed particle momentum has to be consistent with the energy deposit in the calorimeter.

By taking the BigBite to 1.5 meter drift, extra space is available before the magnet to build shielding and to install collimators. Parasitic background tests for the BigBite spectrometer has been planned in Hall A in the coming year, and improvements on the design of the detectors and shielding are expected. In addition, several other experiments are planning to use the BigBite before this experiment starts. Knowledge on the background will certainly help this experiment to improve the shielding and the tracking algorithm.

3.5 The hadron arm spectrometer HRS_L

In addition to the standard tracking and trigger detectors, the hadron arm HRS_L will also have two aerogel Cherenkov detectors, a gas Cherenkov detector, and two layers of lead-glass calorimeter blocks. The aerogel detectors A1 (n=1.015) and A2 (n=1.055) will provide clean π^-/K^- separation [28], their momentum thresholds are shown in Fig. 16. The gas Cherenkov (efficiency $\approx 99\%$) and the lead-glass detectors (efficiency $\approx 99\%$) will provide clean electron identification [29].

Based on data collected during E94010, we estimated that in this experiment the single π^- rate in HRS_L will be at a few kHz level, single electron rate will also be at the kHz level.

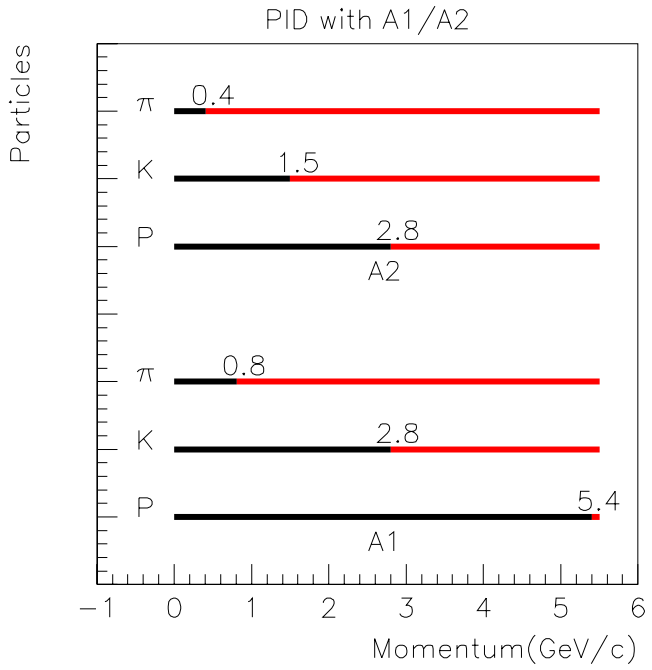

Figure 16: The Cherenkov thresholds for pions, kaons and protons in the two aerogel detectors.

3.6 Trigger, data aquisition and offline event selection

A coincidence time window of 50 ns will be enough to form the coincidence trigger. Trajectory corrected time-of-flight resolution is expected to be about 2 ns. The raw accidental coincidence rate will be at the 500 Hz level, caused by (e, p) or (π^-, p) accidentals. After the BigBite calorimeter ADC cut and the HRS_L gas Cherenkov veto cut, accidental coincidence events are not expected to survive. Two-arm vertex consistency cut is expected to further eliminate the accidental events, by an additional factor of 10, if there is any left. The true $(e, e'\pi^-)$ coincidence event rate is expected to be at a few Hz level when all x-bins are summed over.

As a backup plan, the HRS_L single arm trigger will have the gas Cherenkov sum signal available as an option for electron veto in the trigger. On the BigBite side, the preshower and shower sum signal will also be made available, and could be added to the electron-arm trigger as an option.

Parked at an angle of 90° the right side HRS spectrometer will be run in a parasitic mode as an independent luminosity monitor collecting data through a separated data aquisition system.

3.7 The polarized ^{3}He target.

The Hall A polarized ^{3}He target was successfully used for the experiments E94-010 [30] and E95-001 [31] in 1998-1999, and E99-117 [32] and E97-103 [33] in 2001. The polarized ^{3}He target uses optically pumped rubidium vapor to polarize ^{3}He nuclei

via spin exchange. For a 40 cm long target with target density corresponding to 10 atm at 0°C, average in-beam target polarization is about 42% with beam current of 10-15 μA. Two kinds of polarimetry, NMR and EPR (Electron-Paramagnetic-Resonance), are used to measure the polarization of the target. The uncertainty in the polarization is less than 4%.

Currently, with two sets of Helmholtz coils, the target can be polarized along any direction in the horizontal plane. Two sets of diode lasers ($\approx$ 100 watts each) and optics are used to polarize the target along the longitudinal and the transverse directions. For this experiment, one additional set of coils will be added for the vertical direction. With 3 sets of coils, target polarization along any direction will be possible. The horizontal coils will be oriented to avoid interference with the spectrometer entrances and the beam line, as shown in Fig. 9. The target cell will be kept in the same shape as the current configuration except for the pull-off tip and the placement inside the scattering chamber. While the target chamber (lower chamber) will be kept unchanged, the pumping chamber (upper chamber) will be tilted 45° to the beam right. The oven for the pumping cell will be modified to be offset with a connection piece to link with the original target ladder. The motion and target ladder system will be kept as it is now with a minor modification of an extension rod to keep the motor and any parts containing magnetic material further away from the target field region. A mirror will be mounted on top of the pumping cell such that the laser light will be reflected into the pumping cell from the top. Another set of mirrors will be placed such that the second laser beam line goes into the pumping cell at 45 degrees off the vertical direction. The mirrors will be chosen to be polarization-preserving mirrors as the ones used in E95-001. A schematic of the target system is shown in Fig. 17 for the side view and the view from beam.

The target spin needs to be flipped frequently to minimize systematic effects. To flip the target spin, the holding field needs to be rotated adiabatically and a half wave plate needs to be inserted or extracted to reverse the laser light polarization direction. Currently rotating the field by 180° takes about 5 minutes due to the limitation of the digital electronic control system. During the Los Alamos muon capture experiment, the spin direction was flipped every two minutes [34]. With modification in the electronics, we expect to be able to rotate the holding field in less than 1 minute. The insertion of a half wave plate can also be accomplished in 1 minute. In summary, the spin flip can be done within about 1 minute, and we plan to flip the spin once every hour.

The target polarization will be measured with both NMR and EPR once every few hours. For NMR measurements, the target spin will be rotated to be along the beam direction. EPR measurements can be performed without change in the target spin direction.

The BigBite magnet will be 1.5 meters away from the target center. Its fringe field can cause a field gradient in the target region. We plan to use a field clamp, similar to the design of E02013, to suppress the field gradient. A 1 cm thick μ-metal plate will be enough to shield the target region from the BigBite field. One needs

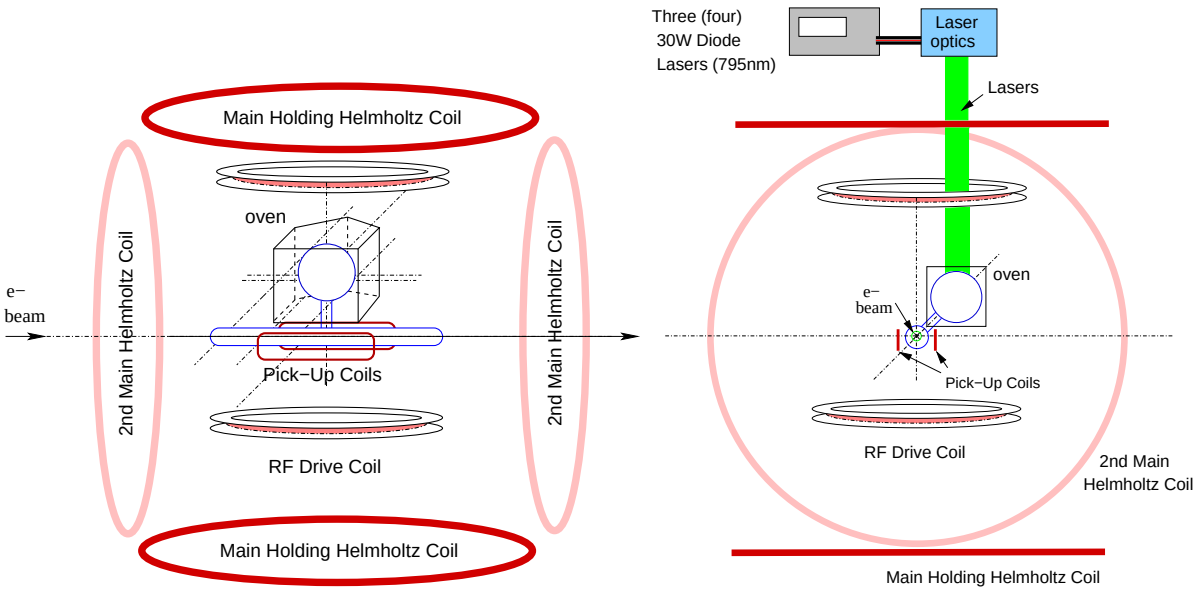

Figure 17: The schematic of the polarized ^{3}He target, side view (left) and beam view (right).

also to consider the effect of the induced field of the field clamp from the Helmholtz coils. Recently, to deal with fringe field from the septum magnets for the E97-110 [35] experiment, we performed Tosca calculations and also performed test measurements with a steel plate placed at various locations away from the target. The calculation as well as the test measurements show that for a field clamp placed at 1.3 meters away from the target center, the induced field gradient is less than 30 mG/cm, which should have a negligible effect on the target polarization. To further reduce the field gradient, and to make minimal polarization loss due to AFP flip during a polarization measurement, two pairs of active correction coils will be installed (as in E97-110), which are expected to be able to reduce the field gradient down to the 10 mG/cm level.

The polarized target system has gone through upgrades and improvements constantly. All the numbers we used for our rate estimate are based on achieved performance. We expect the target to perform even better.

4 Rate Estimate and Beam Time Request

4.1 Cross section and rate estimate

The model of coincident cross sections has the following inputs:

- The inclusive $^3He(e,e')$ cross section.
- A parameterization of the fragmentation functions $D^+(z)$ and $D^-(z)$.

- A model of the transverse momentum distributions of pions as fragmentation products.

The inclusive deep inelastic (e, e') cross section can be expressed in the quark parton model as:

$$\frac{d^2\sigma}{d\Omega dE'} = \frac{\alpha^2(1+(1-y)^2)}{sxy^2}\frac{E'}{M_N\,\nu}\sum_{q,\bar{q}} e_q^2 f_1^q(x), \tag{9}$$

where $s = 2E\,M_N + M_N^2$. The unpolarized quark distribution functions $f_1^q(x)$ and $f_1^{\bar{q}}(x)$ are taken from the CTEQ5M global fits [36]. The semi-inclusive $(e, e'h)$ cross section relates to the quark fragmentation function $\mathrm{D}_q^h(z)$ and the total inclusive cross section σ_{tot} through:

$$\frac{1}{\sigma_{tot}}\frac{d\sigma(e,e'h)}{dz} = \frac{\sum_{q,\bar{q}} e_q^2 f_1^q(x) D_q^h(z)}{\sum_{q,\bar{q}} e_q^2 f_1^q(x)}. \tag{10}$$

For the light quark fragmentation functions $D^+(z)$ and $D^-(z)$, close to $Q^2 = 2.5$ GeV^2, we follow the parameterization of Kretzer, Leader and Christova [37]:

$$\begin{aligned} D^+(z) &= 0.689 z^{-1.039}(1-z)^{1.241} \\ D^-(z) &= 0.217 z^{-1.805}(1-z)^{2.037} \end{aligned} \tag{11}$$

Existing data indicate that the fragmented products follow a Gaussian-like distribution in transverse momentum. For the $N(e, e'\pi)X$ reaction, recent HERMES preliminary data showed that the pion transverse momentum ($P_\perp$) distribution follows the form of $e^{(-aP_\perp^2)}$ with $a = 3.76$ (GeV/c)$^{-2}$, corresponding to an average quark transverse momentum of $\langle P_\perp^2 \rangle = 0.26$ (GeV/c)^2. We used this pion distribution and realistic spectrometer acceptances in a Monte Carlo simulation to estimate the count rates. The issue of pion decay is considered in the rate estimation, typical survival factors for a pion after a flight-path of 25.0 m in HRS$_L$ are 0.78 for p_π=1.8 GeV/c and 0.83 for p_π=2.4 GeV/c.

4.2 Beam time request

The beam time is chosen such that the statistical accuracies in the measured raw asymmetry in the $x = 0.24$ bin is $\approx 0.21\%$. Table 2 lists the beam time request. Table 3 lists the coincidence rates, total number of events, the statistical accuracies of the raw asymmetry A_T(He) and the corrected asymmetry $A_T(n)$ in each x-bin.

5 Expected Results

5.1 From the ^{3}He asymmetry to the neutron asymmetry

Raw measurements of ^{3}He $(e, e'\pi^-)$ single spin asymmetry need to be converted to the neutron asymmetry. We have:

$$A_T(^3He) = P_{^3He} \cdot (f_n \cdot \eta_n \cdot A_T(n) + 2 f_p \cdot \eta_p \cdot A_T(p)) \tag{12}$$

Table 2: Beam time request.

P_{HRS} (GeV/c)	Time (Hour)
1.80 (two target spin settings)	$125 \times 2 = 250$
2.40 (one target spin setting)	290
Time on Pol. ^{3}He Cell	**540**
Time on Reference Cell	15
Optics and Detector Check	5
Target Spin Rotation and Polarization Measurement	15
HRS_L Momentum Change	1
Total Time Request	**576 (24 days)**

Table 3: Estimated coincidence rates, total number of coincidence events, statistical accuracies of raw asymmetry $A_T(^3\mathrm{He})$ and corrected asymmetry $A_T(n)$ in each $\Delta x = 0.05$ bin for two HRS_L momentum settings. The average x values for each bin are listed. The rates are based on 15 μA beam on a 40 cm long polarized ^{3}He target. For the P_{HRS}=1.8 GeV/c setting, statistics corresponding to only one target spin settings are listed. Data from the two target spin settings of this kinematics will be combined to produce the final statistical uncertainties.

$\langle x \rangle$	0.19	0.24	0.29	0.34
two target spin settings	P_{HRS}=1.8 GeV/c (for each spin setting)			
Rate (Hz)	0.58	0.45	0.34	0.25
Number of event (k)	260	204	149	112
$\delta A_T(^3\mathrm{He})$ ($\pm\%$)	0.20	0.22	0.25	0.29
$\delta A_T(n)$ ($\pm\%$)	1.5	1.7	1.9	2.3
one target spin setting	P_{HRS}=2.4 GeV/c			
Rate (Hz)	0.27	0.22	0.18	0.13
Number of event (k)	282	232	183	136
$\delta A_T(^3\mathrm{He})$ ($\pm\%$)	0.19	0.21	0.23	0.27
$\delta A_T(n)$ ($\pm\%$)	1.3	1.5	1.6	1.9

This conversion requires the inputs of:

- the ^{3}He target polarization, which is about $P_{^3He} \approx (42 \pm 4)\%$;
- f_n and f_p: the effective polarization of the proton and the neutron within the ^{3}He nucleus;
- the dilution factor η_n and η_p which is defined as: the ratio of $(e, e'\pi)X$ events on neutron (or proton) over the total $^3He(e, e'\pi)X$ events.

The admixture of S$'$ and D states complicates the nucleon polarization in ^{3}He. The effective nucleon polarization has been computed using three-body Fadeev calculation [38]. In deep inelastic scattering reactions, especially at the valence region of $x = 0.2 \sim 0.3$, one expects: $f_n = 0.86 \pm 0.02$ and $f_p = -0.028 \pm 0.004$.

The yield of $p(e, e'\pi^-)X$ reaction at each kinematics will be quickly measured with the reference cell which will be filled with hydrogen gas at a pressure of ≈ 10 atm. From the yield ratio of $p(e, e'\pi^-)X$ vs ^{3}He$(e, e'\pi^-)X$, dilution factors η_n and η_p can be determined easily to a statistical accuracy of a few percent. At $z \approx 0.5$, one expects that $\eta_n \approx 0.32$ and $\eta_p \approx 0.34$.

Not only the proton has a 3% polarization in ^{3}He, the $A_T^{\pi^-}(p)$ asymmetry is also expected to be small, supported by the existing HERMES data. We used a numerical model calculation [21], and confirmed that the correction on $A_T^{\pi^-}(n)$ in this experiment due to the contribution of $A_T^{\pi^-}(p)$ is indeed negligible. Therefore, as a rough guidance, we have: $A_T^{\pi^-}(^3He) \sim 0.13 A_T^{\pi^-}(n)$.

5.2 Single-spin asymmetry

The expected statistical accuracies of neutron single-spin asymmetry measurements are shown in Fig. 18. The different curves in the figure are predictions which consider the contributions from the Collins effect only, with the assumptions of:

- u–quark only and $h_{1n}^u = g_{1n}^u$, with $h_{1n}^d = 0$;
- d–quark only and $h_{1n}^d = g_{1n}^d$, with $h_{1n}^u = 0$;
- both u–quark and d–quark contribute, with $h_{1n}^u = g_{1n}^u$ and $h_{1n}^d = g_{1n}^d$;
- at the Soffer's bound, with $|h_{1n}^u| = (f_{1n}^u + g_{1n}^u)/2$ and $|h_{1n}^d| = (f_{1n}^d + g_{1n}^d)/2$.

As an illustration, the extraction of raw asymmetry $A_T(^3\text{He})$, for the case of $z = 0.56$ $x = 0.34$ point, is shown in Fig. 19.

Sources of systematic uncertainties that contribute to the raw $A_T(^3\text{He})$ asymmetry would likely come from target spin correlated luminosity fluctuations. To the first order, this type of fluctuation can be largely canceled out by weighting each coincidence event with the instantaneous single electron rate obtained from the "clean" spectrometer.

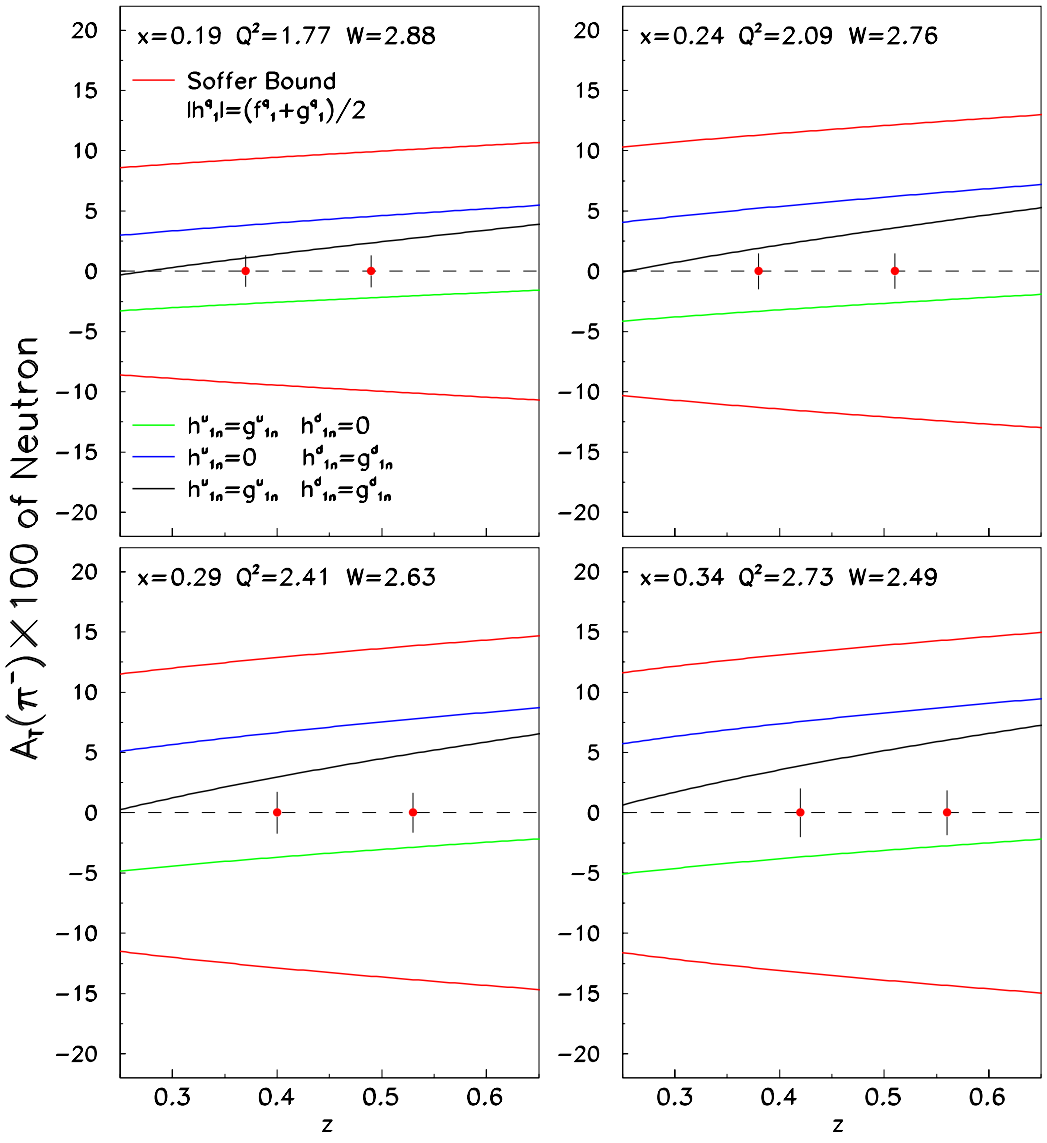

Figure 18: Expected statistical precision for $\vec{n}(e, e'\pi^-)X$ measurements.

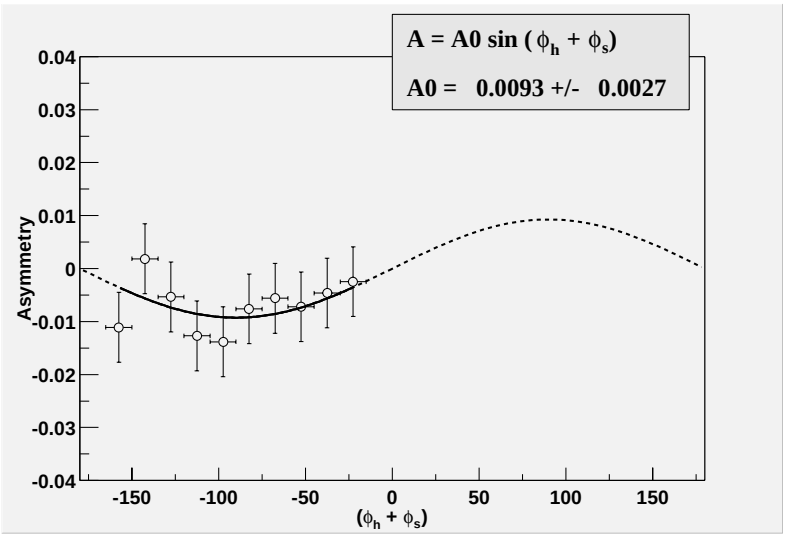

Figure 19: An illustration of raw asymmetry $A_T(^3\mathrm{He})$ extraction for the case of $z = 0.56$ $x = 0.34$ point, assuming the Collins effect dominates the asymmetry. The angles are taken as $\phi_h^l = 180° \pm 50°$ and $\phi_S^l = 90° \pm 25°$. The input of the 1.0% raw asymmetry corresponds to the assumption of $h_{1n}^u = 0$, $h_{1n}^d = g_{1n}^d$. A statistical significance of 3.7σ can be achieved on the asymmetry determination in this illustration.

In $(e, e'\pi)$ reactions, the effects of radiative corrections are expected to be less serious than in the inclusive scattering. In addition, radiative corrections will not generate any single spin asymmetry at the leading order. Therefore, the effect of radiative corrections in this experiment is the alteration of the average values of kinematic variable.

5.3 By-products

As by-products, charged kaon yields are expected to be about at the 10% level compared to the pion yields. Target single spin asymmetries of $\vec{n}(e, e'K^-)X$ reaction will be extracted. Coincidence data will also produce double-spin asymmetries A_{LT} on the $\vec{n}(e, e'\pi^-)X$ reaction, which is sensitive to the quark distribution of g_{1T}. In single arm $(\vec{e}, e')$ data, inclusive asymmetries on a transversely polarized target are sensitive to g_T ($g_T = g_1 + g_2$, which is very sensitive to the higher-twist effects.

Events in higher-x region can be reconstructed from calorimeter alone and asymmetries can also be extracted with less statistical accuracies. Events in the lower-x region, with a lower Q^2 but a higher W can also be used to extract asymmetries.

6 Relation with other experiments

There will be an intense experimental effort aimed at measuring quark transverse polarization in the nucleon in the near future by many collaborations around the world [39]:

- HERMES run–II plans to take data during the period of 2002–2006. Two years of time will be dedicated to the transversely polarized proton target run to measure SSA. Unlike the CEBAF machine, in which the beam helicity can be flipped at a rate of 30 Hz, the positron beam helicity at HERA can not be flipped as frequent, introducing systematic uncertainties in luminosity when the single spin asymmetries are formed.

- Transverse single spin asymmetry measurements are also among the main physics goals of the fixed target COMPASS experiment at CERN [40]. COMPASS uses polarized muons of 100–200 GeV scattering off polarized proton and deuteron targets. These measurements will determine the transversity to $\sim 10\%$ level in the intermediate-x region.

- In the future plans of the ELFE and TESLA-N projects, transversity measurements, which include single-spin azimuthal asymmetries and two-pion correlations [41], represent a significant part of the physics program.

- At the Brookhaven National Laboratory, with an average center-of-mass energy of 500 GeV, the spin-physics program at RHIC will study reactions involving two polarized proton beams with both longitudinal and transverse spin orientations. Transversity distributions are to be studied through Drell-Yan lepton pair production mediated by γ^* or Z^0. However, since the transversity of sea quarks are involved, the expected Drell-Yan double-spin asymmetries are at the $1 \sim 2\%$ level [42].

At the Jefferson Lab, efforts are also underway to consider single spin asymmetry measurements in Hall B using a transversely polarized NH_3 target with 6 GeV beam. The technical difficulties involved in running a transversely polarized target within CLAS are the major challenges to such a physics program. Analysis of the existing eg1a data of Hall B, with a beam energy of 4.2 GeV and a longitudinally polarized NH_3 target, has indicated noticeable single spin asymmetries on the proton [43].

In summary, probing quark transverse polarization is among the goals of several ongoing and future experiments. The experimental study of transverse polarization distributions, which is now only at its inception, promises to have a rather exciting future. Understanding the transversity distributions for different quark flavors is certainly a complex task which demands the collection of a large amount of experimental data in many different reaction channels spanning a wide kinematic range.

7 Summary

This experiment is the first effort in Jefferson Lab to measure the transverse target single spin asymmetry. The precision data on the neutron from this experiment, when combined with the proton data from HERMES and COMPASS, will provide

powerful constraints on the transversity distributions on both u–quark and d-quark in the valence region.

On the technical side, running this experiment in Hall A requires no additional hardware, except those already under development for the approved Hall A G_E^n experiment (E02013). If the two experiments can be scheduled to run next to each other, no major installation time is needed. The only hardware change this experiment requires is the addition of an extra set of target Helmholtz coils and the alternation of laser optics.

We believe that this experiment will have strong physics impacts and yet demands a rather modest investment from the Lab. The success of this experiment will guide the way for the future transversity measurements at the upgraded JLab. A total of 24 days of beam time is requested at 6 GeV.

Appendix: HERMES preliminary data on the deuteron

For completeness, the HERMES preliminary single spin asymmetry results on a longitudinally polarized deuteron target are shown in Fig. 20. Single spin asymmetries are clearly noticeable, but the contributions from the neutron can not be clearly identified by comparing the deuteron data with the proton data as shown in Fig. 21.

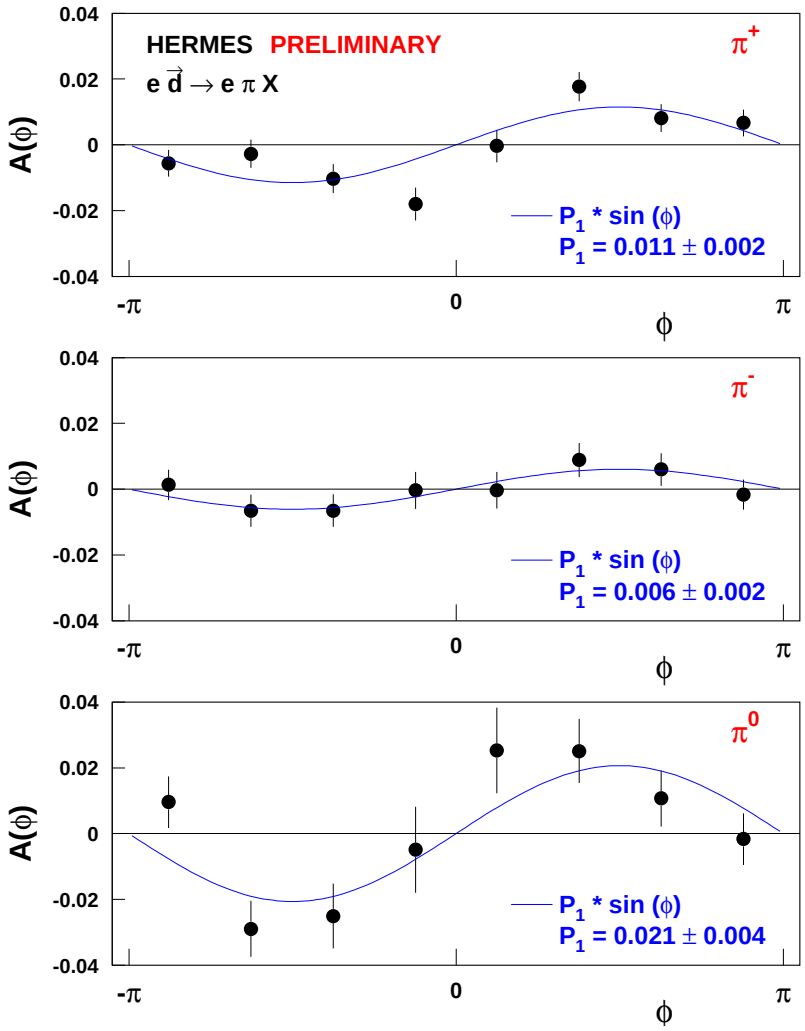

Figure 20: Analyzing power as a function of ϕ from HERMES [2,3] deuteron target measurements.

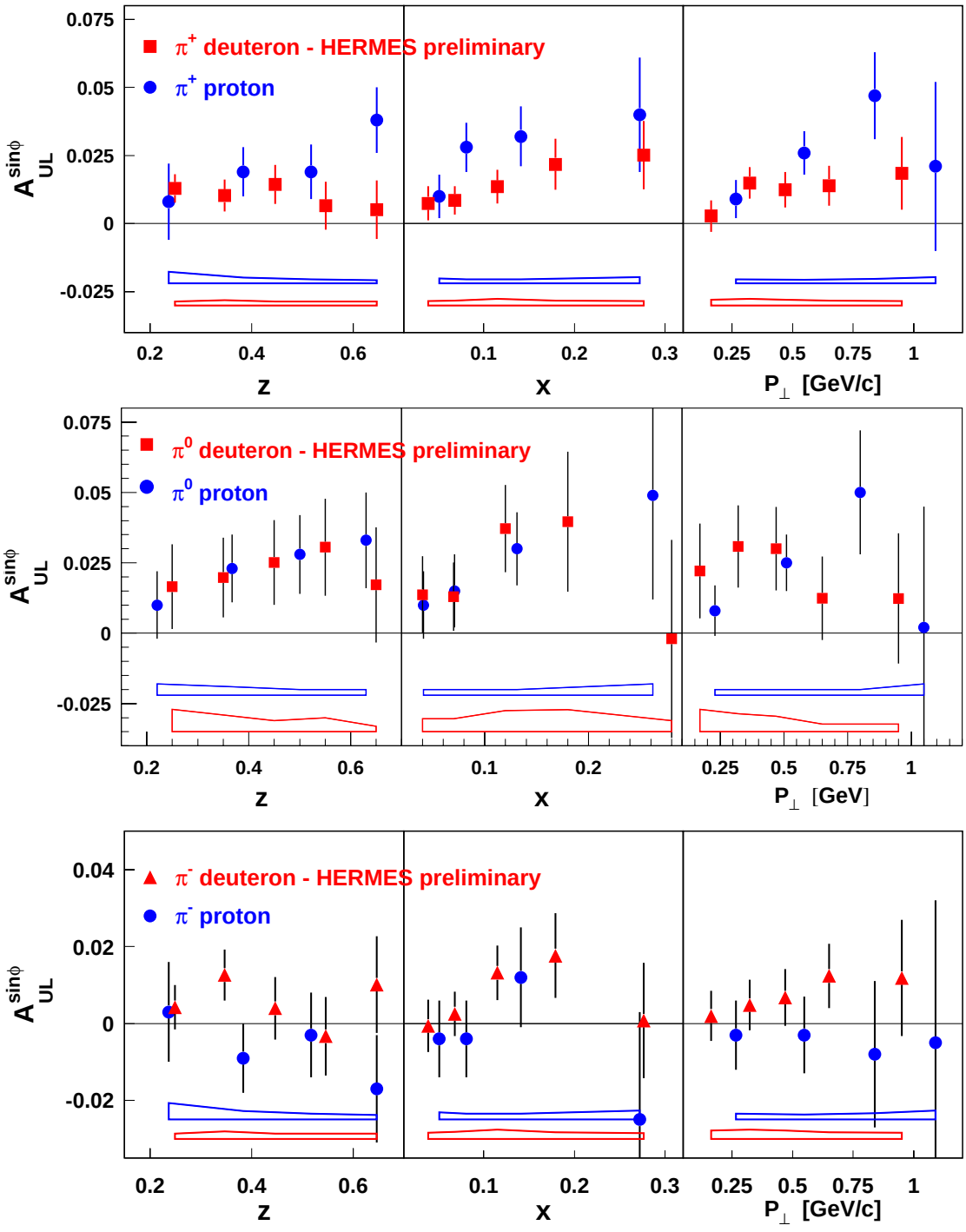

Figure 21: Analyzing power in the $\sin\phi$ moment from HERMES proton [2,3] and deuteron [44] target measurements. Error bars include the statistical uncertainty only. The bands at the bottom of the panels represent the systematic uncertainties.

References

1. See the recent review by V. Barone, A. Drago and P.G. Ratcliffe, *Phys. Rept.* **359** 1 (2002).
2. HERMES Collaboration, A. Airapetian *et al.*, *Phys. Rev. Lett.* **84**, 4047 (2000).
3. HERMES Collaboration, A. Airapetian *et al.*, *Phys. Rev.* D **64**, 097101 (2001).
4. V.A. Korotkov, W.-D. Nowak and K.A. Oganessian, *Eur. Phys. J.* C **18**, 639 (2001).
5. R.L. Jaffe, Proceedings of "Deep inelastic scattering off polarized targets, Physics with polarized protons at HERA", Hamburg/Zeuthen 1997, p. 167-180, Report MIT-CTP-2685, hep-ph/9710465.
6. J.P. Ralston and D.E. Soper, Nucl. Phys. **B 152** (1979).
7. C. Bourrely, J. Soffer and O. V. Teryaev, Phys. Lett. **B420** (1998) 375, hep-ph/9710224.
8. J. Soffer, *Phys. Rev. Lett.* **74**, 1292 (1995).
9. J.C. Collins, *Nucl. Phys.* B **396**, 161 (1993); *Nucl. Phys.* B **420**, 565 (1994).
10. A.V. Efremov, O.G. Smirnova and L.G. Tkachev, Nucl. Phys. Proc. Suppl. **74**, 49 (1999).
11. A. Bravar for the SMC Collaboration, Nucl. Phys. Proc. Suppl. **79**, 520 (1999).
12. P. Mulders and R. D. Tangerman *Nucl. Phys.* B **461**, 197 (1996)
13. A. Kotzinian, *Nucl. Phys.* B **441**, 234 (1995).
14. D. Boer and P. Mulders, *Phys. Rev.* D **57**, 5780 (1998)
15. E. De Sanctis, W.-D. Nowak and K. A. Oganessian, *Phys. Lett.* B **483**, 69 (2000).
16. K. A. Oganessian, H. R. Avakian, N. Bianchi and A. M. Kotzinian, hep-ph/9808368.
17. Stanley J. Brodsky, Dae Sung Hwang and Ivan Schmidt, *Phys. Lett.* B **530**, 99 (2002).
18. J.C. Collins, *Phys. Lett.* B **536**, 43 (2002).
19. D. Sivers, *Phys. Rev.* D **43**, 261 (1991).
20. X. Ji and F. Yuan, *Phys. Lett.* B **543**, 66 (2002). A.V.Belitsky, *et al.*, hep-ph/0208038.
21. Bo-Qiang Ma, Ivan Schmidt and Jian-Jun Yang, *Phys. Rev.* D **65**, 034010 (2002), and hep-ph/0209114.
22. A. M. Kotzinian, *et al.*, hep-ph/9908466.
23. G. Cates, K. McCormick, B. Reitz and B. Wojtsekhowski, Jefferson Lab experiment E02-013: "Measurement of the Neutron Electric Form Factor G_E^n at High Q^2" (2002).
24. P. J. Mulders, hep-ph/0010199.
25. T. Sloan, G. Smadja and R. Voss, *Phys Rep.* **162**, 45(1988).

26. P. Degtiarenko, private communications, November 2002.
27. B. Wojtsekhowski, private communications, November 2002.
28. L. Zhu, Ph.D. thesis of Hall A experiment E95001, MIT, in preparation.
29. K. Slifer, Ph.D. thesis of Hall A experiment E94010, Temple University, in preparation.
30. JLab E94-010, Spokespersons, G. Cates, J. P. Chen and Z. E. Meziani; M. Amarian *et al.*, accepted for publication in Phys. Rev. Lett. (2002) Nucl-ex/0205020;
31. W. Xu, *et al.*, *Phys. Rev. Lett.* **85**, 2900 (2000), and F. Xiong, *et al.*, *Phys. Rev. Lett.* **87**, 242501 (2001).
32. JLab E99-117, Spokespersons, J. P. Chen, Z.E. Meziani and P. Souder; http://hallaweb.jlab.org/physics/experiments/he3/A1n/index.html.
33. JLab E97-103, Spokespersons, T. Averett and W. Korsch; http://hallaweb.jlab.org/physics/experiments/he3/g2/temp/
34. N. R. Newbury *et al.*, *Phys. Rev. Lett.* **67**, 3219 (1991).
35. JLab E97-110, Spokespersons, J. P. Chen, A. Deur and F. Garibaldi; http://hallaweb.jlab.org/physics/experiments/he3/gdh/index.html.
36. H. L. Lai, *et al.*, *Phys. Rev.* D **55**, 1280 (1997).
37. S. Kretzer, E. Leader and E. Christova, *Eur. Phys. J.* C **22**, 269 (2001).
38. C. Ciofi degli Atti, S. Scopetta, E. Pace, and G. Salme, *Phys. Rev.* C **48**, 968 (1993).
39. Proc. of *Future Transversity Measurements* (BNL, September 2000), D. Boer and M. Grosse Pederkamp (eds.), Report BNL–52612.
40. G. Baum *et al.* (COMPASS collab.), COMPASS: A Proposal for a Common Muon and Proton Apparatus for Structure and Spectroscopy, CERN preprint CERN-SPSLC-96-14 (March 1996).
41. R.L. Jaffe, X. Jin, and J. Tang Phys. Rev. Lett. **80** (1998) 1166; Phys. Rev. **D 57** (1998) 5920.
42. G. Bunce, N. Saito, J. Soffer and W. Vogelsang, Ann. Rev. Nucl. Part. Sci. **50**, 525 (2000).
43. H. R. Avakian, presentation at the UVa spin physics workshop, April 2002.
44. HERMES Collaboration preliminary results (http://www-hermes.desy.de).